THESIS FOR THE DEGREE OF LICENTIATE OF ENGINEERING

Towards UWB microwave hyperthermia for brain cancer treatment

Massimiliano Zanoli

Department of Electrical Engineering
Chalmers University of Technology
Gothenburg, Sweden, 2021

Towards UWB microwave hyperthermia for brain cancer treatment

Massimiliano Zanoli

This thesis has been prepared using LaTeX.

Department of Electrical Engineering
Chalmers University of Technology
SE-412 96 Gothenburg, Sweden
Phone: +46 (0)31 772 1000
www.chalmers.se

Printed by Chalmers Reproservice
Gothenburg, Sweden, February 2021

Abstract

Despite numerous clinical trials demonstrating that microwave hyperthermia is a powerful adjuvant modality in the treatment of cancers, there have been few instances where this method has been applied to brain tumors. The reason is a combination of anatomical and physiological factors in this site that require an extra degree of accuracy and control in the thermal dose delivery which current systems are not able to provide. All clinical applicators available today are in fact based on a single-frequency technology. In terms of treatment planning options, the use of a single frequency is limiting as the size of the focal spot cannot be modified to accommodate the specific tumor volume and location. The introduction of UWB systems opens up an opportunity to overcome these limitations, as they convey the possibility to adapt the focal spot and to use multiple operating frequencies to reduce the power deposition in healthy tissues.

In this thesis, we explore whether the current treatment planning methods can be meaningfully translated to the UWB setting and propose new solutions for UWB microwave hyperthermia. We analyze the most commonly used cost-functions for treatment planning optimization and discuss their suitability for use with UWB systems. Then, we propose a novel cost-function specifically tailored for UWB optimization (HCQ). To solve for the HCQ, we further describe a novel, time-reversal based, iterative scheme for the rapid and efficient optimization of UWB treatment plans. We show that the combined use of these techniques results in treatment plans that better exploit the benefits of UWB systems, yielding increased tumor coverage and lower peak temperatures outside the target. Next, we investigate the design possibilities of UWB applicators and introduce a fast E-field approximation scheme. The method can be used for the global optimization of the array parameters with respect to the multiple objectives and requirements of hyperthermia treatments. Together, the proposed solutions represent a step forward in the implementation of patient-specific hyperthermia treatments, increasing their accuracy and precision. The results suggest that UWB microwave hyperthermia for brain cancer treatment is feasible, and motivate the efforts for further development of UWB applicators and systems.

Keywords: microwave hyperthermia, treatment planning, brain cancer.

List of Publications

This thesis is based on the following publications:

[A] **Massimiliano Zanoli**, Hana Dobšíček Trefná, "Suitability of eigenvalue beamforming for discrete multi-frequency hyperthermia treatment planning". *Submitted to Medical Physics*, 2020.

[B] **Massimiliano Zanoli**, Hana Dobšíček Trefná, "Combining target coverage and hot-spot suppression into one cost function: the hot-to-cold spot quotient". *15th European Conference on Antennas and Propagation*, 2021.

[C] **Massimiliano Zanoli**, Hana Dobšíček Trefná, "Iterative time-reversal for multi-frequency hyperthermia". *Physics in Medicine & Biology*, 2020.

[D] **Massimiliano Zanoli**, Hana Dobšíček Trefná, "Optimization of microwave hyperthermia array applicators using field interpolation". *2019 IEEE International Symposium on Antennas and Propagation and USNC-URSI Radio Science Meeting*, 2019.

Other publications by the author, not included in this thesis, are:

[E] **Massimiliano Zanoli**, Mikael Persson and Hana Dobšıcek Trefná, "Self-calibration algorithms for microwave hyperthermia antenna arrays". *12th European Conference on Antennas and Propagation*, 2018.

Contents

Part I

Overview

CHAPTER 1

Introduction

Cancer represents the second leading cause of death worldwide [1]. While the survival rates for most types of cancer have seen a steady improvement over the past decades, certain tumor types seem to have been excluded from this positive trend. For instance, cancers of the central nervous system, the pancreas, the bowel and the lungs [2]. The brain in particular remains one of the most challenging sites to treat, as expressed by an extremely low 5-years survival rate of 22% in the 20-44 age group [3]. Together with short life expectancy, currently available brain cancer therapies are also associated with potentially severe long-lasting side effects. Survivors often experience seizures, walking difficulties, speech problems, and a wide range of others disorders for the rest of their lives [4]. The situation is worse in pediatric patients, where brain tumours are the second most common form of cancer after leukaemia. Modern therapies can cure more than 75% of all children struck with cancer [5], but they entail severe acute and long-lasting side effects. Even low doses of ionizing radiation to the brain can cause cognitive impairment as well as growth disorders [6]–[8]. Therefore, there is a strong need for complimentary therapies with low toxicity that can reduce the amount of radiation administered to the patient without compromising the treatment outcome.

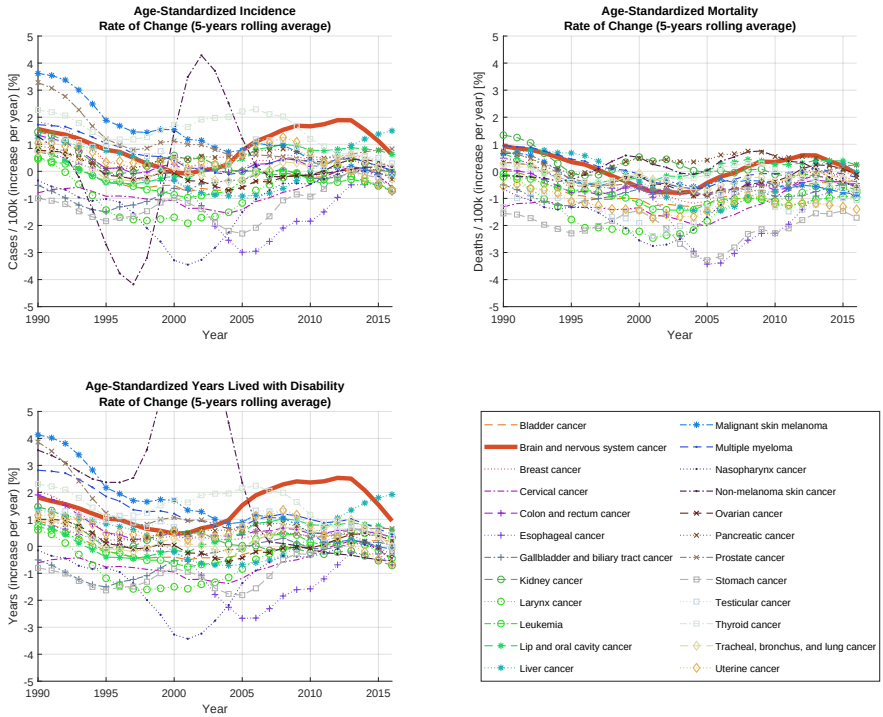

Figure 1.1: Overall age-standardized rate of change of the cancer-related incidence, mortality and amount of years lived with disability considering patients all over the world over the past 30 years. The trend for brain and nervous system cancers is highlighted in solid **red**. While the absolute incidence of these cancers is lower compared to other types, the relative figures indicate that this measure is increasing for brain cancers. In particular, the quality of life of brain cancer survivors, unlike most other patients, has never really improved over the last decades, as shown by the bottom left figure.

Hyperthermia appears to be an ideal candidate for this purpose. After a number of results below expectation in the 1980s followed by a period of skepticism [9], caused mostly by technological limitations and lack of knowledge over the complex, temperature-dependent biological mechanisms in the human body, this form of thermal therapy has seen a major revival in the past decade [10]. Recent meta-analyses and reviews have managed to collect an impressive amount of literature documenting its positive adjuvant effects when applied in combination with radio- or chemo-therapy [11]–[14]. These analyses have demonstrated a significant increase in tumor control probability and even survival rate in some cases with no added toxicity [15], [16]. Yet, to date only few clinical trials have seen the application of microwave hyperthermia as a treatment modality for brain tumours, albeit with encouraging results [17]–[19]. The reason behind this lack of confidence is the imperfect technology used to accurately deliver the prescribed thermal dose in the proximity of critical organs. For instance, in the glioblastoma study [19], despite the improved clinical outcome, homogeneous therapeutic temperatures were difficult to achieve with the interstitial methods used. Thanks to the exponential growth of computational capabilities and development of microwave technology for communication purposes, today we are able to simulate with far greater accuracy the scattering of high-frequency electromagnetic waves inside the body and provide better control of the radiation during treatment. This enables the design of external antenna arrays capable of focusing the heat selectively into the tumour, thus achieving thermal therapy in its most sophisticated form: deep microwave hyperthermia for brain cancer treatment.

1.1 Thesis concept

Intracranial heating is a demanding task. In order to achieve high thermal doses and complete tumor coverage in such a delicate area, microwave hyperthermia systems have to be refined in all their parts to reach the necessary accuracy and precision. Today's loco-regional systems, which are successfully employed in the treatment of abdomen, extremities and neck cancers, rely on a single and fixed operating frequency. This choice comes with many benefits, such as the possibility of being implemented via a simple and robust RF design, but it also involves some limitations. The main constraint of single-frequency systems is the inability to adapt the size of the focal spot to the

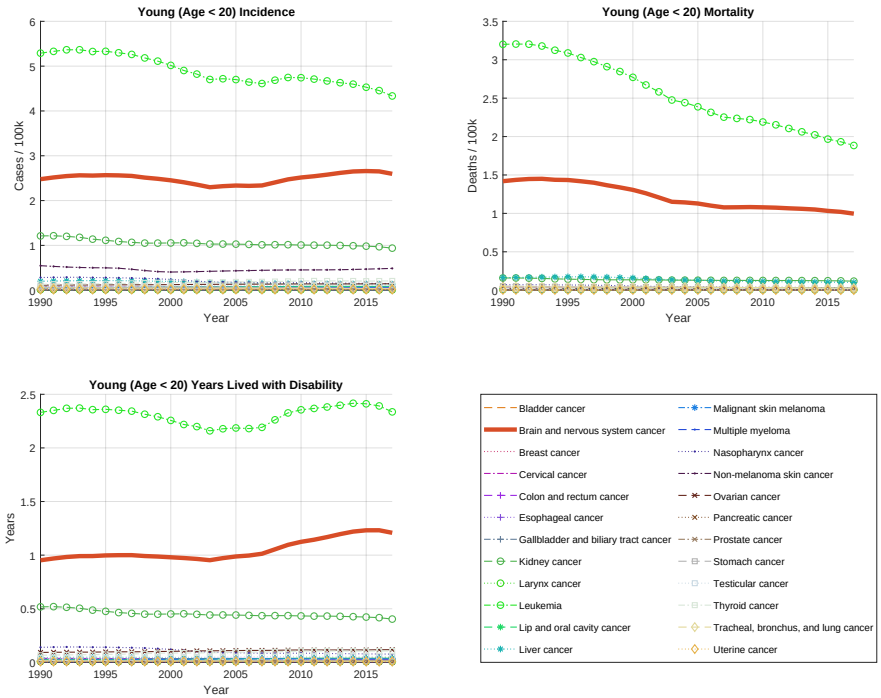

Figure 1.2: Cancer-related incidence, mortality and amount of years lived with disability considering young patients all over the world over the past 30 years. The trend for brain and nervous system cancers is highlighted in solid **red**. Brain tumours are the most common solid-type cancers in children, but unlike leukemia, their incidence has not been decreasing over the past decades. A slight improvement in mortality rates has however led to a huge increase in the amount of years spent with disabilities for these patients, indicating a strong need for therapies with lower toxicities and less after-treatment complications.

particular tumor size and location. We strongly believe that UWB systems are necessary to fulfill the rigorous requirements of microwave hyperthermia treatments in the brain, since they introduce a new degree of freedom in the formation of the power deposition pattern inside the body. The shift towards USB systems is however not trivial, and it implies a revision of hyperthermia treatment planning algorithms, together with a careful redesign the RF steering systems. A second limitation comes from the antenna array applicators, which nowadays are meant to target a body region rather than a particular tumor. In our opinion, a generic applicator will always struggle to reach optimal heating patterns in brain cancer patients, due to the added difficulties in the treatment of this site. A paradigm shift in the applicator design is thus necessary: from regional applicator arrays to target-specific ones. Exploring possible array designs and validating them for each case, however, is a challenging task. Fast array simulation techniques and treatment planning methods are necessary to let us survey all the possible combinations of antennas and frequencies for a specific patient. In this thesis we focus on the development of fast UWB treatment planning algorithms and on the design of (patient) specific (brain) applicators, which will help addressing these questions.

1.2 Thesis outline

This thesis is organized as follows. In Chapter 2, the concept of hyperthermia therapy is introduced along with a brief summary of the main challenges faced and current clinical implementations. Then the scope is narrowed down to the application of microwave hyperthermia (MW-HT) for deep-seated tumours. The implications of moving towards a UWB setting on the applicator design and treatment planning optimization are subsequently explained, and the potential benefits of UWB treatments for brain cancer are discussed.

Chapter 3 begins with an overview of the challenges faced in electromagnetic and thermal modelling. The treatment planning (TP) phase of MW-HT, which is extensively based on computer simulations, is described and several approaches to this problem are discussed. The author's novel contribution of a iterative time-reversal method for TP is reported and compared to the clinical standard and to other solutions reported in the literature.

The investigations carried out on how to put together an optimal antenna

array applicator for MW-HT are reported in Chapter 4. Here, the design of the array is discussed under the UWB perspective. A field interpolation technique to quickly evaluate many potential array configurations is described and utilized to propose a number of nearly-optimal applicator designs for a specific patient and tumour anatomy. The method is further applied to the specific case of a medulloblastoma patient and a promising helmet applicator design is obtained by means of global optimization.

Chapter 5 includes a discussion on the hardware needed to implement such a helmet applicator and describes the challenges and ongoing efforts of manufacturing a robust MW-HT system for head, neck and brain cancer treatment. The chapter ends with conclusive remarks and a layout of future work. The author's paper contributions are summarized thereafter and are reported at the end of the thesis.

CHAPTER 2

(Microwave) Hyperthermia

Thermal therapy has been known to human kind as a way to treat diseases ever since the ancient times. In many examples throughout history, physicians attempted, often successfully, to cure diseases by means of induced fever or burn malignancies with incandescent sticks or blades [20]. Heat is also a fundamental component of the body's natural self-defense mechanisms. Local and systemic responses, triggered by the presence of pathogens, are often associated with inflammation or fever, implying a temperature increase in the tissue or body, respectively. In the past, the temperature rise was seen as a mere consequence of the increased metabolic activity necessary for the fight, but nowadays this is no longer the general view among immunologists. In fact, it has become more and more evident that the elevated temperature has a role in itself, enhancing the activity and efficacy of our immune system, even in the absence of pathogens [21].

With time, researchers have unveiled a number of microscopic and macroscopic, local and systemic, biological and physiological effects of heat and elevated temperature on the body [22], [23]. These mechanisms point towards a strong therapeutic potential of artificial temperature elevation in the treatment of cancers and other diseases. Treatment methods relying on the external

administration of heat are nowadays divided into two categories: thermal ablation and *hyperthermia*. The aim of the first is to kill the tumor cells by literally burning them, which requires temperatures > 45 °C. The method is highly localized and carried out by means of invasive procedures [24]. Modern mild hyperthermia for cancer treatment, on the other hand, is defined as the elevation of the tumor temperature to $40 \sim 44$ °C [25]. This range of temperatures has been shown to trigger a number of mechanisms at a molecular and tissular level that considerably improve the tumor response to traditional cancer therapies such as radio- and chemo-therapy [26], [27], Fig. 2.1. Hyperthermia is thus seen today as a potent adjuvant modality to these two main practices, and its inclusion has been shown to enhance survival rate and tumor control probability for a number of cancer types [10]–[13], [16].

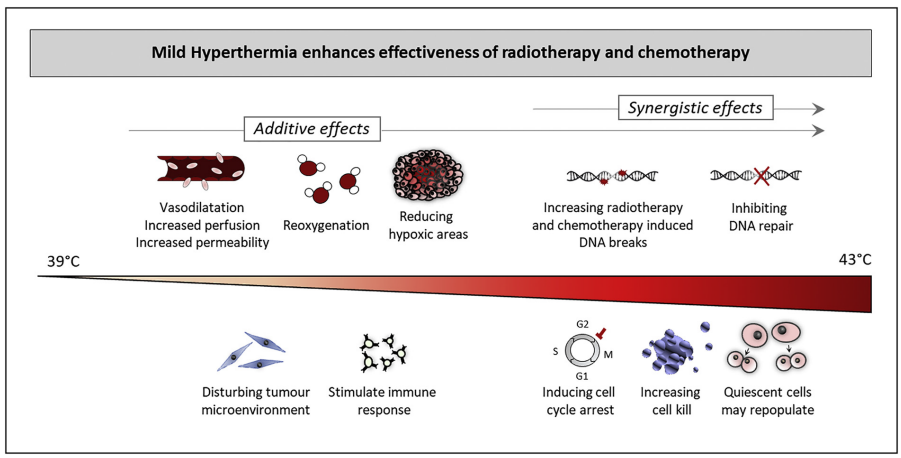

Figure 2.1: Summary of the additive and synergistic effects of mild hyperthermia on radiotherapy and chemotherapy, from [28]. Vasodilation increases blood perfusion resulting in deeper penetration of chemotherapeutic agents; increased oxygenation enhances the induction of DNA breaks by radio-therapy; disturbances in the tumour micro-environment stimulate the immune responses; inhibition of the DNA repair mechanisms enhances the damage provoked by radio- and chemo-therapy.

Unfortunately, the optimal temperature of 43 °C, as suggested by biological studies [28], [29], is usually not achieved inside the target in clinical practice [30]. The reason behind this is the imperfect technology utilized in delivering

the prescribed thermal dose to the target volume [31]. From a biomedical engineering perspective, the task of reaching a predefined and controlled temperature distribution in a biological tissue *in-vivo* is indeed a challenging task. The ability of living organisms to maintain their homeostasis is extraordinary and the body will use all means to counteract the artificially administered heat. As soon as the local temperature deviates from the set level of 37 °C, blood perfusion and sweating increase to remove the excess heat. This response is non-linear and can vary significantly from patient to patient. This renders external heat delivery a demanding technique whose implementation requires careful and robust design. On top of this, the monitoring of the actual temperature distribution inside the patient during treatment, necessary for the assessment of the thermal dose, is by no means a trivial task [32]. All these aspects have to be taken into account and addressed for when designing a reliable system for hyperthermia treatments.

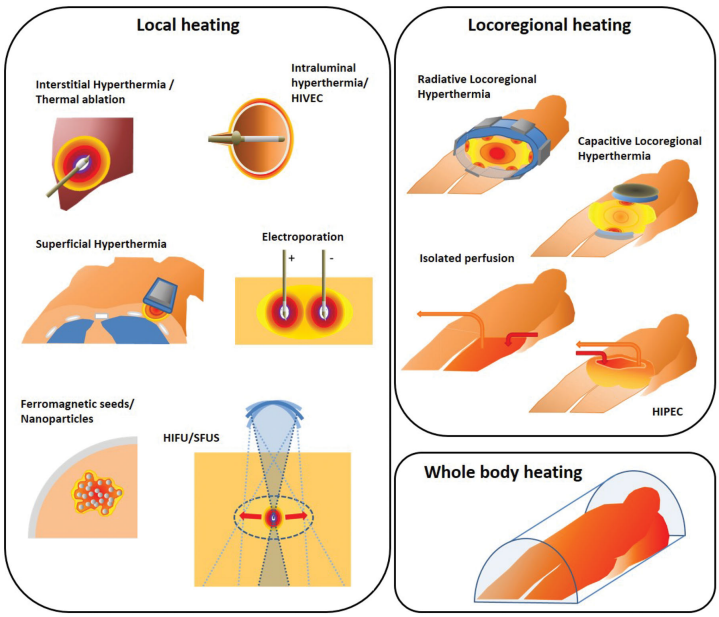

Figure 2.2: Graphic summary of the techniques available for the administration of the thermal dose in hyperthermia treatments, from [33].

The list of technologies available today to deliver hyperthermia is long [33], Fig. 2.2. However, only few of them have been applied in the treatment of brain tumors. Among the techniques proposed in the past two decades to selectively induce a temperature increase [34], only interstitial hyperthermia, magnetic nano-particle hyperthermia and high-intensity focused ultrasound (HIFU) have been clinically applied to deep seated brain tumors. Interstitial hyperthermia combined with brachytherapy applied to high-grade glioblastomas has been demonstrated to be a safe and attractive modality to improve the survival of these patients [35], [36]. Despite the promising results in terms of an improved treatment outcome, homogeneous tumor temperatures were difficult to achieve with the interstitial applicators used. More recently, the use of magnetic fluid hyperthermia to enhance heating precision was investigated [37]. Results demonstrated an increase in tumor temperatures and higher overall survival than conventional therapies [38], [39]. The disadvantage of this technology lies, however, in the direct injection of iron oxide nanoparticles into the tumor. These nanoparticles can remain in the treated area for a lifetime, thus hindering the patient from undergoing future MRI scans, which is, despite the (minimally) invasive procedure, a clear limitation of this technique. HIFU provides localized energy delivery through small volumetric sonifications from an ultrasound phased array transmitter to destroy intracranial lesions by thermocoagulation [40]. Heating of large volumes, as is usually the case for childhood brain tumors, is nevertheless still demanding with the present technology. Furthermore, ultrasound based treatments suffer from high energy losses in the bone structures, and despite novel technical solutions, its implementation in the brain will very likely be limited to tumors located centrally and at a distance from the skull [41].

Microwave hyperthermia, which relies on the non-invasive deposition of focused EM energy into the tumor by a phased array of antennas [14], [25], has the potential to circumvent these limitations and achieve therapeutic temperatures in brain tumors without the need for surgical interventions [42]. However, several technological challenges must first be resolved to provide the centimeter-scale spatial control needed to compensate for vascular cooling in living tissues and to deal with the small anatomical features of the head. The typical setup for a non-invasive microwave hyperthermia treatment is shown in Fig. 2.3. The patient lies on a treatment bed or chair and a so-called applicator is placed around the region to be treated. The applicator consists of

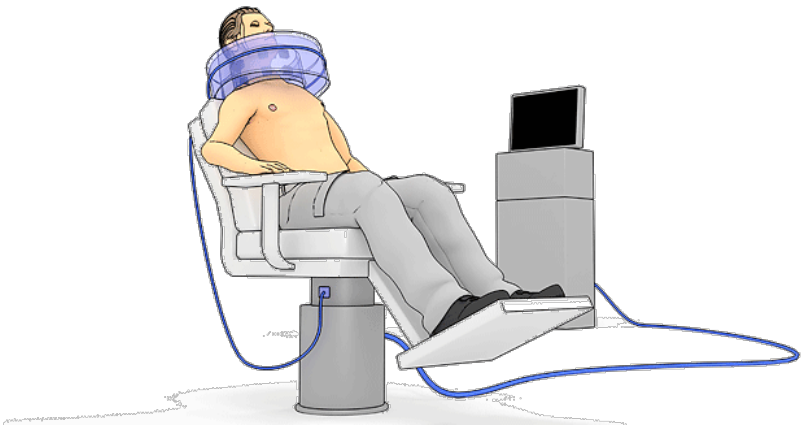

Figure 2.3: Microwave hyperthermia for cancer treatment, conceptual drawing.

a phased array of antennas and a water bolus. The water bolus has two purposes: to realize an impedance match between the antenna and the patient, and to cool the skin and dampen superficial hot-spots. Each channel of the applicator array is independently steered in amplitude and phase, to shape the interference patter and power loss deposition inside the patient. In the case of a discrete multi-frequency UWB system, each frequency can be steered independently from the others, and the power loss is given by the superposition of the interference patterns at all frequencies. The RF amplifying system must deliver the phase-locked signals with adequate accuracy and precision. Deviations of amplitude and phase in modern hyperthermia systems do not exceed $\pm 5\%$ and $\pm 5°$ respectively from the nominal value [43], [44]. Because of the high power that each channel is supposed to deliver for adequate heating, the antennas must exhibit high directivity and low cross-coupling. Current clinical hyperthermia systems operate over a narrow frequency band, which makes their construction relatively simple. Examples are $70, 100$ MHz for the pelvic and abdominal region [45], [46] and 434 MHz for the head and neck [47]. Of course, if an UWB hyperthermia system is to be deployed, both the antennas and the RF cascade must be adapted to operate across the entire target frequency band. This represents an additional layer of difficulty with respect to the current technology.

Despite the impressive advances that the field of microwave hyperthermia

has witnessed in the past 30 years, present treatments (still) suffer from the inability to adequately heat tumors in several regions that could benefit from this type of therapy. This has resulted, among other things, in the study of Sneed *et al.* [36] being the sole experience with microwave heat delivery into the brain, albeit with promising results. We believe that the lack of accurate thermal dose delivery and reliable temperature monitoring in this region has made it extremely difficult to properly trace a dose-effect relationship. Fortunately, there is mounting evidence that the development of UWB applicators capable of operating at different frequencies can lead to improved target coverage and hot-spot suppression [48]–[50], which might once more motivate efforts for the development of brain applicators [51]–[53].

An UWB system can exploit the complementary interference patterns generated by different frequencies to increase the net average power delivered to the tumor while reducing the absorption in healthy tissues. This is expected to benefit treatments in the brain region, which is characterized by a combination of anatomical and physiological factors that require an extra degree of accuracy in the formation of the heating pattern. The cerebral tissue is more sensitive to deviations in temperature than other tissues [54], and the presence of cerebrospinal fluid can cause strong and treatment-limiting hot-spots to appear in the immediate vicinity of the brain. Yet, recent developments suggest that an implementation of microwave hyperthermia for brain cancer treatment is within reach [42]. To conquer the trust of the oncologists and the medical community, however, real clinical evidence is necessary. A crucial precondition to successful clinical trials, in turn, is the development of reliable hyperthermia systems and robust treatment planning methods. In the following chapters, we discuss how treatment planning optimization algorithms can be extended into the UWB domain, and how these can be used in the design of UWB-optimized applicators for brain cancer treatment.

CHAPTER 3

Treatment Planning

Treatment planning is a fundamental stage of microwave hyperthermia treatments [55]. It consists in several steps aiming at determining the set of steering parameters that yield high temperatures in the tumor while sparing the surrounding healthy tissues from excessive heat, Fig. 3.1. In the case of deep hyperthermia administered by phased array applicators, the steering parameters are the amplitude and phase of each antenna. Varying these settings affects the wave propagation inside the patient and shapes the EM interference pattern and consequent power deposition. Historically, the tuning of the steering parameters in single-frequency applicators with up to a handful of independent steering channels has been performed manually with the help of EM probes [56]. The task is often carried out qualitatively, and with little information about the actual resulting distribution of the power losses inside the patient. The clinical experiences gathered over time, however, revealed that it is crucial to identify the location and severity of power deposition peaks, as these often lead to hot-spots in healthy tissues thereby effectively limiting the maximum achievable temperature in the target [57]. Today, clinical applicators can reach up to 12 independently steered channels [47], and the problem of determining the optimal amplitude and phase settings for each antenna has

become non-trivial. The situation is further complicated if an UWB system is to be deployed: the task of choosing the optimal combination of operating frequencies and their weight in the treatment plan is quite involved and a global optimum is hard to determine [58].

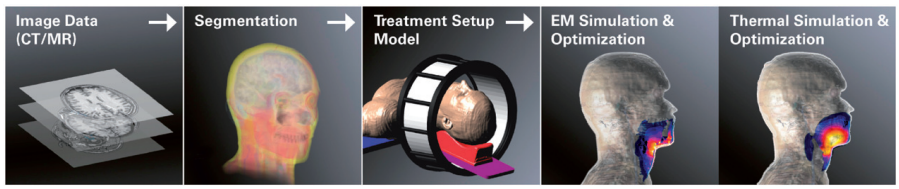

Figure 3.1: Stages of microwave hyperthermia treatment planning, from [59].

Hot-spots can arise in the healthy tissues as these lie in the path between the antennas and the target. As a consequence of their relatively high conductivity at microwave frequencies [60], tissues tend to absorb energy from the traveling wave and heat up. This is aggravated by the anatomical heterogeneity and the presence of sharp interfaces between tissues with different dielectric properties, which cause multiple reflections and localized intensity peaks. The imperfect interference pattern generated by the limited-aperture phased array also contributes to the uneven localization of the energy losses. The threshold temperature for hot-spot related pain complaints is typically $\approx 45\ ^\circ\mathrm{C}$ [61]. However, in the brain, damage and thermal related toxicity can be detected already with temperatures above $\approx 42\ ^\circ\mathrm{C}$ [54]. To manage occurring hot-spots before and during treatment is therefore mandatory. Superficial hot-spots within depths of one to two centimeters from the skin can be suppressed by applying a water bolus circulated with cool water. Hot-spots that arise in deeper locations, however, are more difficult to manage. The sole strategy to suppress or limit those hot-spots is to reduce the power deposition at those locations while preserving the constructive interference (focus) in the target volume. The problem is challenging, but it can be tackled with the help of optimization algorithms.

Tons of methods to determine the optimal amplitudes and phases for an applicator array that yield satisfying target coverage and limited hot-spot temperatures have been reported in the literature and are still subject of ongoing research [59], [62]. These methods can be classified into two main categories: specific absorption rate (SAR) based and temperature (T) based. SAR based

techniques rely on the assumption that the SAR distribution is predictive of the temperature distribution in the patient [63]. However, since the thermal response of the body can be highly non-linear, SAR-based optimizers can yield sub-optimal, while still clinically relevant, steering parameters. T-based optimizers, on the other hand, have evolved to include complex non-linear aspects such as discrete vasculature and systemic response under thermal stress [64]. Ideally, a full implementation of T-based treatment planning in the clinical routine is desirable, since temperature is the objective dose. In current practice, however, the theoretical benefits of T-based optimizations are somewhat diminished due to the lack of accurate estimations of the thermal tissue properties [65]–[67]. These thermal properties, and blood perfusion in particular, exhibit large variations across patients and even at individual level in different treatment sessions. In summary, both SAR-based and T-based approaches are being clinically applied as both require adjustments during treatment in response to hot-spots [57], [68]. Considering the current equivalence of these two approaches, in this thesis we consider only SAR-based treatment planning. The choice is motivated by the fact that SAR-based optimization requires less computational resources, thereby allowing for quicker comparisons among a large number of possible treatment plan solutions.

3.1 Patient modeling

In today's state-of-the-art treatment planning for microwave hyperthermia, virtual patient models are used to simulate the wave propagation in the body in conjunction with the specific applicator model in use [62]. The patient models are obtained from CT or MRI scans and subsequently segmented into a discrete number of tissues [69]. How detailed the segmentation should be, depends on the frequency utilized by the applicator as well as on the region to be treated. A study to determine the impact of the number of segmented tissues in the pelvic region on the SAR distribution revealed the importance of properly representing high water content tissues [70]. On the one hand, the set of segmented tissues must be limited to spare computational resources and avoid over-fitting. On the other hand, all the spatial variations in electromagnetic properties that might affect the wave propagation have to be captured, as well as all critical healthy tissues where a strict temperature limit must be enforced.

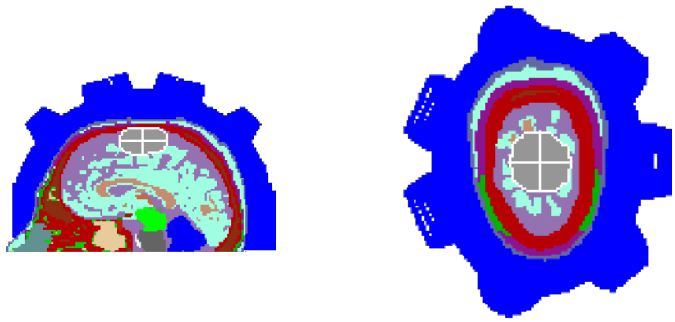

(a) Sagittal **(b)** Transverse

Figure 3.2: Example of a patient model, discretized at a resolution of 2 mm. The model encompasses the upper head and is terminated at the level of the nose to reduce its computational weight. The applicator and water bolus are also included (blue shape). The target, a 30 ml meningioma, is outlined in white.

A second aspect of patient modeling is the resolution. In the pelvic area, for instance, clinical treatment planning tools utilize resolutions of $2.5 \times 2.5 \times 2.5$ mm for both simulation and optimization purposes [57]. Conversely, in the neck region, the current practice is to perform a high-resolution simulation of the wave propagation followed by a lower resolution treatment planning optimization step at $5 \times 5 \times 5$ mm [68], [71]. This is done to keep the computational burden of the optimization process at bay and enable online and real-time readaptation of the steering parameters upon patient complaints. Whether this resolution is sufficient to capture the wave scattering in small anatomical features such as nerves and bones is however uncertain. In intracranial heating, the presence of the skull, whose thickness can be as little as 3 mm [72], is particularly relevant, as bone exhibits notably different dielectric properties than soft tissues. Furthermore, the space discretization carried out for the sake of computer analyses and simulations is usually realized on hexahedral grids. This implies that the maximum allowable voxel size has to be further restricted in order to properly sample the skull's curvature. Another critical issue is the presence of cerebrospinal fluid, since its high conductivity at

microwave frequencies makes this tissue prone to overheating. The interconnected cavities where this fluid is free to move are also characterized by narrow passages and thin strati. Accordingly, all computations in this work have been realized on patient models with resolution $2 \times 2 \times 2$ mm.

The subsequent phase in patient modeling is the assignment of the dielectric and thermal properties to the segmented tissues. As already mentioned, tissue properties exhibit large variations across the population and are in general difficult to obtain for the specific patient. Such variations depend on the person's age [73], fitness level, and other factors. The variation is typically larger for thermal properties than for electromagnetic ones [67]. In addition to the variance across the population, intra-patient variations can also be possible between subsequent treatment sessions. This is due to the body adapting to environmental and behavioral changes to better preserve its homeostasis. Factors that can affect the tissue response include the ambient temperature, the patient's hydration level [74], or whether the patient has carried out any recent physical activity. Finally, most thermal tissue properties, and blood perfusion in particular, are dependent on the local temperature itself [75], [76]. This temperature dependence can strongly affect the hyperthermia treatment plan and ultimately the effectiveness of the treatment. Nevertheless, a useful and relevant estimation of the wave propagation and resulting thermal distribution inside the treated area can still be obtained with a good degree of approximation by relying on tissue property databases with modified perfusion values [65], [77]. The uncertainty in the resulting SAR and temperature distributions due to tissue property variations has been estimated to be around 20 % [78]. In the works reported here, all the healthy tissue properties have been obtained from the IT'IS database [60], which represents a valuable collection of literature values from decades of measurements. To mimic the presence of a tumor, the delineated target volumes have been filled with a material exhibiting properties equal to the weighed average of the materials originally composing the volume. Some thermal properties have been further adjusted to reflect the response of tissues to thermal stress: muscle perfusion is increased by a factor 4 due to the systemic response to heat [76], tumor perfusion is decreased by a factor 0.7 to account for its chaotic vasculature [79], and the thermal conductivity of the cerebrospinal fluid is increased by a factor 10 to emulate the convective transport of heat [42].

3.2 Simulation techniques

The next step in treatment planning optimization is to perform electromagnetic and thermal simulations [59], [62], by inserting the patient model in a virtual model the applicator in use, which also includes the water bolus. The first simulation computes the E-field and power loss distributions generated by each antenna. A number of electromagnetic simulation methods have been described in the literature, either based on the differential or the integral form of Maxwell's equations. The electromagnetic field distribution can be calculated using either the finite-difference time-domain (FDTD) method or the finite-element (FEM) method. Both methods have seen wide application in biomedical engineering. Generally speaking, the FDTD method is more frequently used in hyperthermia treatment planning as it relies on hexahedral grids which are easier to interface with patient voxel models. To avoid reflections of the electromagnetic waves at the boundaries of the computational domain, several variations of absorbing boundary conditions can be used. Among them, the perfectly matched layer [80] is considered as the the most effective. Once the E-field distributions are available, the resulting power loss distribution relative to each operating frequency is calculated by superposition after steering each channel in amplitude and phase according to the treatment plan (Section 3.4). The electromagnetic energy of the traveling wave is converted into heat as a consequence of the lossy nature of the tissue. The amount of energy absorbed in each point can be described by the SAR distribution, which measures the power loss per unit mass of tissue:

$$\mathrm{SAR}_f = \frac{1}{2}\frac{\sigma_f}{\rho}|E_f|^2 \tag{3.1}$$

where σ_f is the tissue conductivity at frequency f, ρ is the tissue density, and E_f the total electric field at this frequency. In a multi-frequency treatment plan, the overall power deposition can be obtained as the sum of the single frequency components:

$$\mathrm{SAR} = \mathrm{SAR}_1 + \mathrm{SAR}_2 + \ldots + \mathrm{SAR}_f \tag{3.2}$$

The resulting temperature distribution inside the patient is estimated by means of a second, thermal simulation where the SAR term is included as a distributed heat source. The standard thermal modelling in hyperthermia

treatment planning is based on Pennes' bioheat equation [81]:

$$\rho c \frac{\partial T}{\partial t} = k\nabla^2 T + \omega \rho_B c_B (T_B - T) + Q + \frac{\mathrm{SAR}}{\rho} \tag{3.3}$$

where ρ is the tissue's density, c the tissue's specific heat capacity, T the temperature, t is time, k is the tissue's thermal conductivity, ω is the tissue's blood perfusion coefficient, ρ_B is the blood's density, c_B is the blood's heat capacity, T_B is the blood's temperature, and Q is the heat generated by the tissue's metabolic activity. In the term representing the externally applied heat, the SAR is converted into volumetric power loss density (PLD). Pennes' equation describes the tissue's thermal behavior as a first-order dynamic system. By setting the time derivative on the left-hand side to zero, the steady state temperature distribution can be obtained, which shows the predicted location of hot spots and tumour temperatures. On this distribution, the temperature-based hyperthermia treatment quality indicators can be evaluated (Section 3.3) and the treatment's viability can be decided. In this work, the well established commercial software CST Microwave Studio® is used for both electromagnetic and thermal simulations [82].

3.3 Treatment planning quality indicators

The goal of hyperthermia treatments is to achieve the prescribed thermal dose in the entire clinical target volume. For this to be possible, the thermal dose has to be defined with a quantitative measure. Since the therapeutic effect is reached by a combination of temperatures above 40 °C and prolonged exposure time, the dose metric has to capture these two notions simultaneously. To this end, the Cumulative Equivalent Minutes at 43 °C (CEM_{43}) metric has been proposed [83] and adopted in clinical trials [84]. The temperature exceeded by x % of the target volume is used as lumped temperature value for the evaluation of the metric, yielding $\mathrm{CEM}_{43}T_x$, where x can be 90 or 50. The applicability of this metric in the context of the actual sub-optimal temperatures achieved in the clinics has been debated, but there appears to be consensus in that the metric represents a good measure of the overall thermal dose [30], [85].

In view of this, the treatment planning stage, where the steady-state temperature distribution is estimated and optimized, should aim at maximizing

the temperatures in all parts of the tumor, with the only constraint of the maximum tolerable temperature in healthy tissues. According to the $\mathrm{CEM}_{43}T_x$ definition, we can assess the steady-state distribution using precisely the temperature indicators T_{90} and T_{50}. These, in turn, have been shown to correlate with the SAR-based indicators TC_{50} and HTQ when applied retrospectively to clinical data sets [86], [87]. These indicators are defined as follows:

- **HTQ**: hot-spot to target quotient [88]:

$$\mathrm{HTQ} = \frac{\overline{\mathrm{SAR}}_{\mathrm{R1}}}{\overline{\mathrm{SAR}}_{\mathrm{T}}} \tag{3.4}$$

  i.e. the ratio between the average SAR in the sub-volume containing the highest 1-percentile SAR among the remaining tissues ($\overline{\mathrm{SAR}}_{\mathrm{R1}}$) and the average SAR in the target volume ($\overline{\mathrm{SAR}}_{\mathrm{T}}$). Values of HTQ around or below 1 are typically considered for clinical treatment.

- **TC_x**: iso-SAR target coverage [89]:

$$\mathrm{TC}_x = \frac{V_{\mathrm{T}}(x)}{V_{\mathrm{T}}} \quad , \quad V_{\mathrm{T}}(x) \;\mid\; SAR[V_{\mathrm{T}}(x)] \geq x \cdot SAR[V] \tag{3.5}$$

  i.e. the fraction of the target volume V_T where SAR values are above a given fraction x of the SAR peak value in the whole patient volume V. Both the TC_x value and the fraction x are usually expressed as percentage, and the TC_x index is evaluated in this work for $x = 25$ % or $x = 50$ % depending on the model at hand. Values of TC_{25} greater than 75 % are typically considered for clinical treatment.

This correlation enables the use of SAR as a surrogate for the temperature distribution during the treatment planning optimization process, thereby saving in model complexity and computational resources. In particular, TC_{25} has been shown to directly correlate with clinical outcome [89].

However, point SAR, as given in Equation 3.1, has little value in terms of temperature prediction. In fact, Pennes' equation (3.3) acts as a spatial low-pass filter on the heat sources, while the SAR distribution is evaluated at the individual grid points and can therefore exhibit sharp changes at the tissue interfaces. Consequently, if the SAR distribution has to be used as surrogate for the temperature, the point SAR has to be smoothed according

to some averaging scheme. For instance, in SAR exposure standards for mobile phones and other body-contact RF devices, the evaluation of absorption peaks is carried out over a mass-averaged SAR distribution [90]. This approach is also adopted in hyperthermia treatment planning, and the averaging scheme involves the use of a convolution kernel whose size is increased until the mass of patient tissue within reaches a specified amount. The SAR values outside the patient are excluded from the average, thus preventing surface hot-spots from being potentially overlooked. The amount of averaging mass is however a matter of debate [91]–[94]. The consensus for low, non-medical exposures seems to lie on 10 g, which is also adopted in technical standards. For higher thermal doses, 1 g SAR mass averaging seems to be a better predictor of the temperature distribution [95]. During our internal evaluations, we noticed that the 1 g-based hyperthermia treatment optimization in the brain region leads to higher tumor temperatures than a 10 g-based one. Once again, this might be a result of the particular anatomy of the head, where the skull ($\approx$ 6 mm, [72]) is adjacent to a thin layer of skin ($\approx$ 5 mm, [96]) on one side and cerebrospinal fluid ($\approx$ 4 mm, [97]) on the other. All these tissues exhibit considerably different dielectric and thermal properties. In a rough estimation, assuming the kernel to be cubic and its contents homogeneous, the averaging cube for cortical bone ($\rho \approx 1900$ Kg/m^3, [60]) would be of side $\approx$ 1.7 cm in the 10 g case and $\approx$ 8.1 mm in the 1 g case . Conversely, in the case of skin or cerebrospinal fluid ($\rho \approx 1000$ Kg/m^3, [60]), the cube side becomes $\approx$ 2.1 cm (10 g) and $\approx$ 1.0 cm (1 g). Of course, where the cube is not entirely filled with a single tissue or part of it lies outside the patient, its size will vary in between these values or increase further. When compared with the anatomical layer thicknesses, these estimations suggest that 10 g averaging is too coarse to capture the location and severity of hot-spots in the superficial areas of the brain region, which absorb most of the incoming wave. Therefore, we opted for a 1 g SAR mass averaging scheme for all the treatment planning optimizations and distribution analyses reported in this work. The averaging scheme is similar to the *CST Legacy* one as described in [98], albeit with a spherical kernel rather than cubic.

3.4 Treament planning optimization

Many approaches to determine the optimal amplitudes and phases for each antenna in the applicator have been proposed, as summarized in excellent reviews [59], [62]. These steering settings aim at maximizing the thermal dose as described in the previous section. In particular, the multiple objectives of the hyperthermia treatment plan optimization problem, i.e. high target temperatures with extensive coverage and limited temperature increase in healthy tissues, are mathematically described by a lumped cost function. Different optimization algorithms, either direct or iterative, are then applied to solve for this cost function.

Cost functions for SAR-based optimization

In a study by Canters *et al.* [63], a number of cost functions for SAR-based treatment planning were summarised and analysed in terms of their correlation with the temperatures achieved in the patient. As a result, the HTQ (Equation 3.4) was proposed and implemented in the clinical routine at the Erasmus University Medical Center, Rotterdam, The Netherlands [86]. Another, widely used, cost function is the target-to-remaining average SAR ratio defined in the early days by Böhm *et al.* [99] as follows:

$$\mathrm{SAF} = \frac{\overline{\mathrm{SAR}}_{\mathrm{T}}}{\overline{\mathrm{SAR}}_{\mathrm{R}}} \tag{3.6}$$

where SAF stands for SAR Amplification Factor, $\overline{\mathrm{SAR}}_{\mathrm{T}}$ is the average SAR in the target, and $\overline{\mathrm{SAR}}_{\mathrm{R}}$ is the average SAR in the remaining healthy tissues. The main benefit of SAF is that a ratio of quadratic polynomials in the unknowns (the steering parameters) can be solved directly using eigenvalue (EV) decomposition. When the resulting SAR (or temperature) distribution is showing overheated healthy regions, a weighing factor can be introduced to iteratively reduce the power deposition at those locations [100], [101]. EV is a direct method that provides a fast and deterministic solution and has therefore been used extensively in clinical hyperthermia treatment planning. However, it is unclear whether solving for the maximum SAF ratio actually yields the highest and most homogeneous possible temperature distribution in the tumour. In fact, the analysis of Canters *et al.* [63] revealed that quadratic cost function predictions correlate poorly with the temperature rise in the tar-

get volume during clinical treatment. Yet, still to date, SAF and EV-based optimization methods are considered a means to evaluate the heating capabilities of an applicator design prior its clinical use [102]–[104]. Furthermore, the role of the SAF ratio as a cost function for multi-frequency UWB treatment planning remains unclear.

We have therefore investigated the suitability of EV and SAF for single- and multi-frequency hyperthermia treatment planning [105], Paper A. We showed that the SAF ratio (3.6) cannot be maximized by more that one frequency at a time. In particular, even when the EV solver is complemented by an iterative optimization procedure that minimizes for another cost function, for instance the HTQ as in [101], the final solution will always consist of only one operating frequency, regardless of how many frequencies are available for concomitant treatment. Is this a problem for deep microwave hyperthermia? Is it a strong limitation to use only one frequency for treatment, as long as this frequency can be selected across a wideband range? Can the use of multiple operating frequencies improve target coverage and hot-spot suppression thanks to their complimentary interference patterns? To answer these questions, we went a step further and analysed two realistic test cases, a tumor in the larynx and a tumor in the meninges. We compared the resulting temperature distributions when a single frequency is used, to the case when two simultaneous frequencies are jointly optimized with respect to their overall SAR distribution. The latter optimization had to be carried out using some other cost function than (3.6) and a solver other than EV (in this case, the Particle Swarm global stochastic optimizer). Results for the larynx indicated that a single frequency treatment is sufficient to reach satisfying values of T_{50} and T_{90} in this region, and that adding a secondary frequency would not improve the thermal distribution further. However, in the brain case, introducing a second frequency would increase SAR target coverage, TC_{50}, by 10 points, and temperature coverage, T_{90}, by 0.5 °C with respect to the best single-frequency solution (from 40.9 °C to 41.4 °C). In terms of $CEM_{43}T_{90}$, such an increase would correspond to a doubling of the thermal dose. This means that multi-frequency systems do have the potential to improve hyperthermia treatments in regions typically difficult to treat such as the brain.

A relevant question to be asked at this point is: if SAF is not an appropriate cost function for treatment planning optimization, what cost function should be used to fulfill all the requirements of hyperthermia treatments and to fully

exploit the potential of multi-frequency systems? At a first glance, the HTQ (3.4) seems to be a promising candidate. The definition of HTQ includes a non-linear term through the evaluation of the highest 1-percentile SAR in the healthy tissues. Because of this, it is not subject to the single-frequency limitation that affects SAF. As mentioned before, HTQ is also used as treatment quality indicator, and the correlation of its inverse, 1/HTQ, with the temperature increase in the target has been shown. However, HTQ is not the sole SAR-based treatment quality indicator. TC_{25} and TC_{50} (3.5) need also be evaluated to determine the viability of a plan prior to treatment. Yet, the relationship between these indicators is not straightforward. It is unclear, for instance, whether they assess contrasting objectives in treatment planning or if their optimal SAR distributions correspond. Furthermore, the limitations of both indicators when used as cost function for treatment planning optimization should be clarified. The HTQ aims at suppressing the most relevant hot-spot in the healthy tissues while raising the average power deposition in the target. Therefore, it does not account for inhomogeneities of the SAR distribution inside the target volume. As a direct implication, a low HTQ value, which would suggest a "good" plan, can be achieved with SAR distributions comprising narrow localized peaks in the tumor, while leaving most of the target volume uncovered and untreated. On the other hand, the TC_x indicator, when used as cost function, aims at extending the SAR coverage throughout the target volume with respect to a fixed fraction of the overall SAR peak inside the patient. This implicitly neglects the possibility to deliver more raw power to the target, i.e. when the SAR in the target can exceed this fixed fraction of the peak.

In view of these considerations, we investigated the relationship between HTQ and TC_{50} [106], Paper B. In this study, we considered the two realistic test cases of the larynx and of the meningioma and obtained the optimal treatment plannings with respect to HTQ and TC_{50} by means of a global stochastic optimizer (Particle Swarm). The results confirmed that the two indicators assess different and not necessarily correlated aspects of the hyperthermia treatment plan. In particular, optimizing for the HTQ often yields too low values of TC_{50}, indicating poor coverage. An parallel issue occurs when optimizing for TC_{50}: the resulting HTQ is systematically high. Values of HTQ above 1 indicate the presence of a prominent hot-spot that may limit the temperatures achieved in the tumor during treatment. Consequently, we

proposed a novel cost function for hyperthermia treatment planning whose aim is to combine the aspects assessed by HTQ and TC_{50} into one metric. The cost function, called the hot-to-cold spot ratio (HCQ), is defined as:

$$HCQ_p = \frac{\overline{SAR}_{Rq}}{\overline{SAR}_{Tp}}. \tag{3.7}$$

where $\overline{SAR}_V$ indicates the average SAR in volume V, while Rq (Tp) represent the q-percentile (p-percentile) sub-volume of healthy (tumor) tissue with highest (lowest) SAR. The relationship between the two percentiles is fixed and defined by:

$$q = p\frac{|T|}{|R|} \tag{3.8}$$

where $|V|$ is the size of the volume V. In this study, the cold-spot percentile p was chosen to be 10 % of the tumor volume. As in the HTQ, the purpose of the hot-spot term in the numerator is to suppress potentially treatment-limiting SAR peaks in the healthy tissues. The cold-spot term in the denominator, on the other hand, makes sure that all areas of the target volume are covered by sufficient SAR deposition for homogeneous heating. The relationship (3.8) guarantees that the HCQ is always normalized to the patient and target volume, rendering values of HCQ from different plans comparable. When used as cost function for the treatment planning optimization of the two realistic test cases, the HCQ revealed a good ability to yield solutions exhibiting both low HTQ and high TC_{50}. Moreover, the HCQ provided consistent results for both single- and multi- frequency settings. More importantly, given a discrete set of possible operating frequencies to choose from, the HCQ-based optimizer could always determine a combination of one or more frequencies that exhibited HCQ and TC_{50} close to their globally optimal values for the examined cases. It could be concluded that the single cost function formula (3.7) provides the means for an effective multi-frequency treatment plan optimization and enables meaningful comparisons between a large number of potential treatment solutions. Naturally, future work should include a thermal validation of the relationship between the HCQ and the thermal indicators T_{50} and T_{90}, ideally on clinical data sets.

Algorithms for optimization

While non-linear cost functions yield more clinically relevant treatment planning solutions than quadratic ones, the price to pay is the impossibility to directly determine these solutions. Unlike the SAF ratio, non-linear cost functions require iterative optimization schemes. In modern clinical planning tools, the optimization is carried out by global stochastic optimizers, mainly Particle Swarm (PS) [107]. Another alternative is the use of genetic algorithms, as they allow for multi-objective optimization [108]. While these solvers can find the global optimum of any given problem with high probability, they suffer from slow execution times, while demanding large computational resources. This drawback conveys relevant limitations for online treatment planning re-optimization, which is mandatory in clinical practice [57]. As discussed above, planning tools based on stochastic optimizers require coarse patient model resolutions to maintain real-time usability. However, for intracranial hyperthermia treatments, denser sampling grids and more detailed patient models are necessary. This calls for faster alternatives to stochastic optimizers. So far, only few UWB solvers have been suggested, with a vast majority of them involving the use of quadratic-programming optimization [50], [53], [109]. As such, these solvers cannot be applied to non-linear cost functions, and neither are they able to return the HCQ-optimal distribution. Consequently, there is a need for fast iterative UWB solvers that can solve for non-linear cost functions.

One promising such method is Time Reversal (TR). TR-focusing is a fast, intrinsically wide-band and deterministic method that has been proposed and validated as an alternative treatment planning optimization technique for microwave hyperthermia [110], [111]. TR processing is a well characterized inverse filter initially developed for focusing ultrasound pulses generated by transducer arrays inside a biological target [112], [113], and subsequently extended for use with electromagnetic antenna arrays [114]. It exploits the time and space reciprocity of the wave equation to determine the optimal phase and amplitude settings of an array of radiators that will cause the highest constructive interference to occur at the desired location. In its basic implementation, with a single virtual source placed at the center of the tumor, TR yields solutions that exhibit good target coverage [49], [111], [115] albeit far from the global TC_x optimum. Further improvements for hot-spot management in TR have been proposed for high-intensity focused ultrasounds

(HIFU), based on iterative methods [116]. In general, the major hindrance for the clinical introduction of TR-based treatment planning optimization is its limited ability to suppress hot-spots.

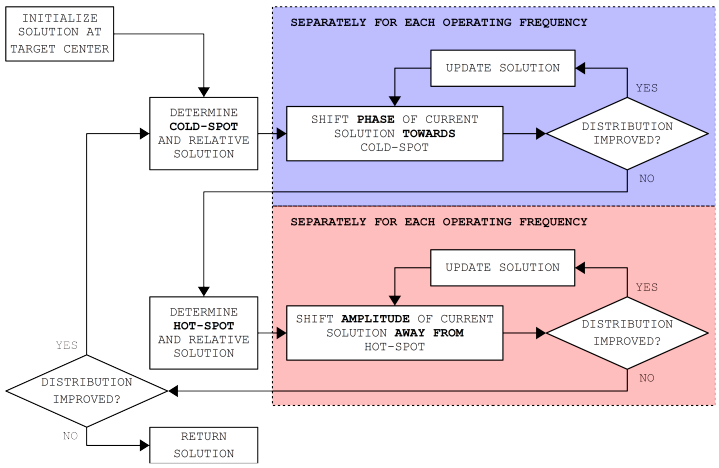

Figure 3.3: Simplified description of the proposed iterative time-reversal scheme. The blue section indicates a set of cold-spot (phase) iterations, while the red section refers to a set of hot-spot (amplitude) iterations.

To improve hot-spot suppression and target coverage in TR-based treatment planning, we proposed a novel deterministic UWB TR-based iterative scheme (i-TR) [117], Paper C. The scheme aims at minimizing the HCQ (3.7) and is specifically tailored to this purpose. The procedure, Fig. 3.3, is initialized at the classic TR solution obtained by placing a virtual source at the center of the tumor mass. The resulting (time reversed) SAR distribution is analysed and the most prominent cold-spot is identified as the p-percentile sub-volume of the target containing the lowest SAR values. A virtual source is placed at the center of the cold-spot and a TR solution for focusing at that location is determined. Similarly, the most prominent hot-spot is identified as the q-percentile sub-volume of healthy tissues containing the highest SAR values. A virtual source is placed at the center of the hot-spot and a TR solution for focusing at that location is determined. The algorithm then selects the first operating frequency in the set and begins improving the current solution by progressively shifting each channel's steering phase towards the phase of the

cold-spot solution. At each step, the HCQ is evaluated over the focused SAR distribution and the new solution is deemed improved if the HCQ exhibits a lower value than the previous. Subsequently, the solution is further improved by progressively shifting each channel's steering amplitude away from the amplitude of the hot-spot solution (i.e., towards the inverse of the hot-spot solution's amplitudes). If the HCQ does not improve, the next frequency in the set is selected and a new attempt is made to improve the solution. Once the HCQ does no longer improve by either a cold- or a hot-spot step at any frequency, the SAR distribution is re-evaluated and a new pair of cold- and hot-spot are identified and their TR solutions computed. The whole procedure is then reiterated until the new set of cold- and hot-spot solutions does not bring any improvement in HCQ. The algorithm then halts and the latest solution with lowest HCQ is returned as the optimized treatment plan.

In this study, we show that i-TR yields results comparable to those obtained via global stochastic optimization, while being significantly faster. The algorithm is benchmarked numerically for two different applicator array topologies: a collar for tumors in the neck and a helmet for tumors in the brain. For the neck model, different target locations and sizes are considered, to assess the algorithm's robustness to different scenarios. The algorithm is also applied to two realistic cases, a tumor in the larynx and one in the meninges. For each test case, treatment planning quality and performance indicators are computed and compared against those obtained with EV, PS and classic (non-iterative) TR. Results suggest that the method is successful in finding viable multi-frequency solutions for a given problem, independently of the target's size, location, morphology or composition. They further indicate that the method is robust to problems involving mixed polarization axes. The quality of the i-TR solution can depend on the selected set of operating frequencies, however the high execution speed makes it possible to evaluate all frequency combinations and always determine one viable solution. The treatment plans obtained via i-TR are further validated with thermal simulations. We verify that i-TR can achieve the same tumor temperatures (T_{50}) as the treatment plans based on global PS-based HTQ optimization. In the larynx case, i-TR outperforms the HTQ-based plan by 0.4 °C, potentially confirming HCQ's suitability as cost function for optimization.

CHAPTER 4

Applicator Design

The electromagnetic energy is delivered to the patient by an antenna applicator. The temperature elevation in deep seated targets is often better achieved with a phased-array, i.e. a set of coherently driven antennas placed around the patient. The antennas are suitably fed in amplitude and phase to create a constructive wave interference to selectively heat the target region. The steering parameters are optimized during treatment planning as discussed in the previous chapter. Currently, all clinically utilized microwave applicators operate at a single frequency and consist of one or more concentric rings of antennas whose polarization is aligned with the symmetry axis [14]. In these applicators, the antennas are immersed in a common water bolus, Fig. 4.1, which fills the gap between the patient and the array. Beyond skin cooling and impedance matching, the water bolus also serves as a high permittivity medium to reduce the antenna size. Several parameters can be varied in this design to achieve the desired power loss distribution pattern, and they have been investigated in many studies [45], [118]–[120].

The design parameters typically include: the operating frequency, the radius of the circular or elliptical arrangement, the number of rings, the number of antennas per ring. The optimal combination of these parameters depends,

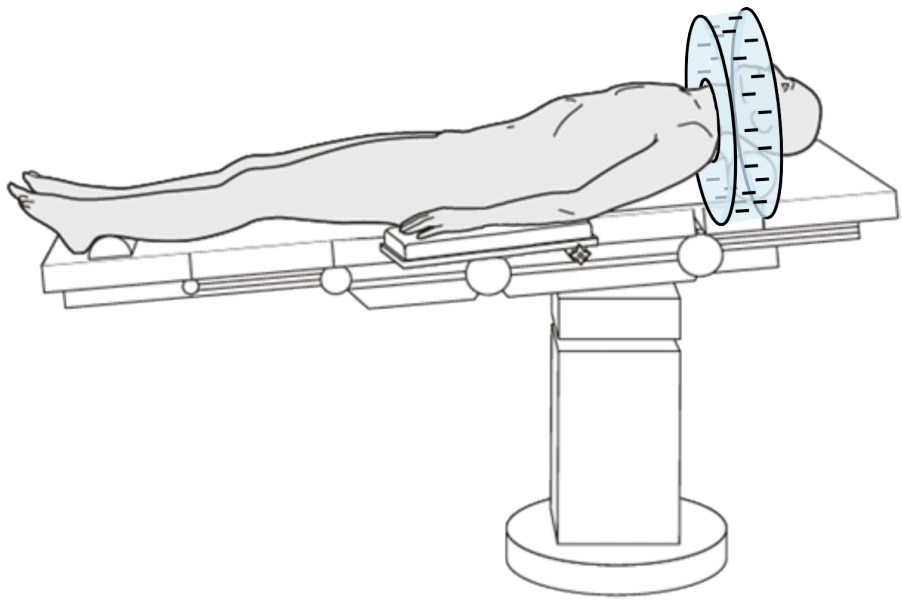

Figure 4.1: Clinical dual-ring applicator design, example in the neck region. The light blue shade represents water. The antennas are indicated with a pin following their main polarization direction.

in a more or less direct manner, on the operating frequency itself. The choice of operating frequency, in turn, determines the size of the resulting focal spot and the penetration depth [121]. For compliance, the operating frequency is usually selected among the limited set of frequencies allocated for medical use in the regulated spectrum. Therefore, the vast majority of systems operate at $434,915$ MHz or 2.45 GHz. Systems deployed for use in shielded rooms can operate outside the ISM bands and utilize lower frequencies for deeper penetration. In the pelvic and abdominal regions, for instance, the typical operating frequency is between 70 and 140 MHz. Accordingly, the consolidated recipe for the design of a single-frequency applicator involves the following steps: 1. determine the operating frequency based on the region to be treated, 2. choose a narrow-band directional antenna at the target frequency, 3. determine the best array arrangement based on the previous constraints (and other external constraints such as space, cost, etc.). The clinical systems used nowadays for treatments of tumors in the pelvic region, the abdomen, and the head and neck, have mostly been designed according to this approach [120].

In the UWB setting, this approach is no longer applicable. The design of UWB systems cannot be based on the target operating frequency, precisely because this is no longer defined. Rather, an *operating band* must be chosen. This band can span more than an octave and is only constrained by external factors, such as the (commercial) availability of RF components and their cost. In fact, in terms of deep microwave heating, the operating band can be located anywhere between ≈ 1 MHz and ≈ 1 GHz. Beyond this limit, the penetration depth of the impinging wave becomes gradually irrelevant and its effect on the body temperature can only be seen within a few centimeters from the skin surface [25]. The actual penetration depth obtained by a conformal array of antennas is higher thanks to the array effect, but similar considerations apply. In general, lower frequencies have to be included to support heating at depth, while higher frequencies can contribute to the spatial refinement of the thermal dose distribution. The microwave hyperthermia system for head, neck and brain treatments that is being developed at Chalmers features 16 channels designed to operate across the $300 \sim 800$ MHz frequency band. The diameter of the smallest achievable focal spot ($\lambda/2$) at 300 MHz is ≈ 5.3 cm in water, while at 800 MHz this diameter is ≈ 2.0 cm.

The possibility to choose any operating frequency within the band adds another degree of freedom in the array applicator design, namely the antenna

size. The ideal antenna for UWB treatments should in fact exhibit the following characteristics:

- high return loss (> 10 dB)
- high directivity (> 10 dB)
- low cross coupling (< -10 dB) between nearby elements
- high operating power (≈ 150 W)
- small size ($< \frac{\lambda}{2}$)

across the entire operating band. Unfortunately, when the target frequency band spans more that one octave, it is nearly impossible for any antenna design to fulfill all these requirements simultaneously. Thus, instead of relying on a single antenna type, one can consider scaled versions of the same octave-antenna to cover different (and possibly overlapping) ranges within the wider operating band of the RF amplifier system. The brain applicator being developed at Chalmers features two sets of antennas, a bigger one working across the $300-600$ MHz range and a smaller one for the $400-800$ MHz range. These antennas are implemented using a self-grounded bow-tie (SGBT) design and exhibit small electrical size and naturally high directivity [122]. The further reduce back-radiation, size and cross-coupling between nearby antennas, each antenna is immersed into a separate water bolus [123], Fig. 4.2a.

In addition to the possibility to choose among different antenna sizes introduced by the UWB setting, the design of an applicator for the brain region allows for yet another degree of freedom. Unlike for other body parts, in fact, the array morphology is not limited to concentric rings of antennas, as visualized in Fig. 4.3a. The array can rather be entirely conformal to form a helmet around the head, fully exploiting the surface available on the scalp, Fig. 4.3b. In terms of heating capability, the inclusion of more antennas at different angles can lead to better tumor coverage [52]. Furthermore, these antennas can be polarized in different directions to compensate for the distortions and irregular wave scattering introduced by the strongly heterogeneous anatomy of this region. In other words, considering the antenna polarization direction as a design parameter might increase the net average power delivered to the target while reducing the entity of SAR peaks in the surrounding healthy tissues.

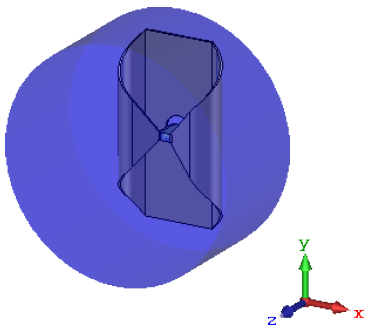

(a) Antenna Model

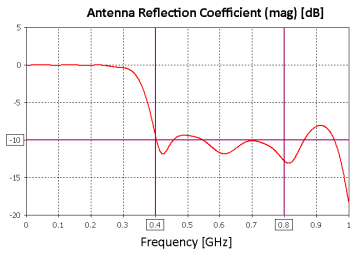

(b) Reflection Coefficient

Figure 4.2: The 400 – 800 MHz SGBT antenna for brain applicators. The blue shade indicates water. b) reports the reflection coefficient when the antenna is applied to a 1 cm thick water bolus surrounding the scalp.

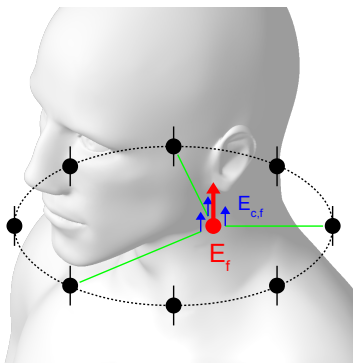

(a) Collar Applicator

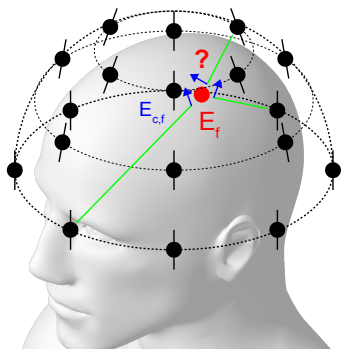

(b) Helmet Applicator

Figure 4.3: Collar versus helmet applicator topology. The antennas are indicated by black pins. The focal spot is indicated with a red dot, and the E-field of each channel at this location is indicated with a red arrow. In the helmet case, the resulting E-field polarization at the focal spot cannot be determined right away, as the antennas contribute each with a different angle to the power deposition at the focus.

As discussed in the previous chapters, the brain region requires extraordinary control in the delivery of heat to avoid damage to life-critical organs. To achieve this accuracy, how many small and big antennas should the optimal brain applicator consist of? How should they be arranged around the head? How should they be rotated to fully exploit the polarization diversity? The commonly used strategies in antenna applicator design, based on single parameter studies, are inadequate to tackle all the additional degrees of freedom. We believe that the logical step forward in applicator design is to combine all the design parameters into a global optimization process. This would consider:

- operating frequency
- number of antennas
- size of each antenna
- location of each antenna
- rotation of each antenna

The goal of the optimization is to find the antenna arrangement that yields maximum target coverage and hot-spot suppression, i.e. high TC_{50} and low HTQ, for a given patient. The optimization can be carried out with a global stochastic optimizer configured to solve for the hot-to-cold spot quotient (HCQ), described in Section 3.4. The number of antennas should always be the highest possible to maximize the array effect and is only limited by the available water bolus surface. At the same time, it is well known that for a given patient and target volume, only a subset of the array is typically active during treatment [103], [124]. This fact allows us to treat the number and size of antennas as fixed design parameters and optimize for the rest. The optimization can then be repeated for a few test sets to qualitatively determine the best compromise for these parameters. Thus, for a given size and number of antennas, the optimization variables are the coordinates of each antenna around the scalp together with its rotation angle. Since all these variables are defined on continuous intervals, they are suitable for use with efficient global and local optimization algorithms. These algorithms are typically iterative, and they require an evaluation of the cost function for a new candidate solution at each step. Since each new solution corresponds to a previously unexplored array configuration, both the E-fields and the steering

parameters have to be determined anew. Ideally, the evaluation of the cost function consists of two stages:

1. Simulate the UWB wave propagation for each antenna in the current array configuration.

2. Determine the HCQ-optimal steering parameters to focus in the target volume and use this HCQ as cost function value.

Step 1 can be particularly time consuming and resource demanding. In a realistic case of a 16-channel UWB applicator, a full array simulation at the appropriate resolution cast last hours with a commercial FDTD scheme, even on a modern GPU. At the same time, a global optimization procedure with 3 variables for each antenna can take up to thousands of iterations to complete. Consequently, for the optimization to be feasible, the evaluation of the cost function should run within minutes. Having developed a fast UWB treatment planning algorithm in Paper C to carry out Step 2 in reasonable time, we need to accelerate the procedure in Step 1. In the next section, we introduce an E-field approximation method that allows for the rapid estimation of the field distribution generated by each antenna at any location and polarization angle around the head.

4.1 Fast E-Field Interpolation and Array Evaluation

In [125], Paper D, we presented a novel field interpolation technique that allows for a quick estimation of the E-field distributions generated by a particular array arrangement at any operating frequency. The interpolation is based on a pre-calculated set of E-field distributions generated by a single antenna at fixed locations around the head, forming an interpolation grid, Fig. 4.4. For each location, two orthogonal polarization directions are simulated. The E-field generated by an antenna at a specific location and rotation is then obtained by a weighed average of the three nearest sampled locations (triangular patch). Note that this approach does not account for cross-coupling effects between nearby antennas, which might affect the power deposition pattern inside the patient. However, thanks to their separate water-boli, the SGBT antennas used in our system exhibit low coupling (< -15 dB). It is therefore

possible to neglect the secondary fields passively generated by nearby resonating antennas and superpose the single antenna distributions to obtain a good estimation of the overall array pattern.

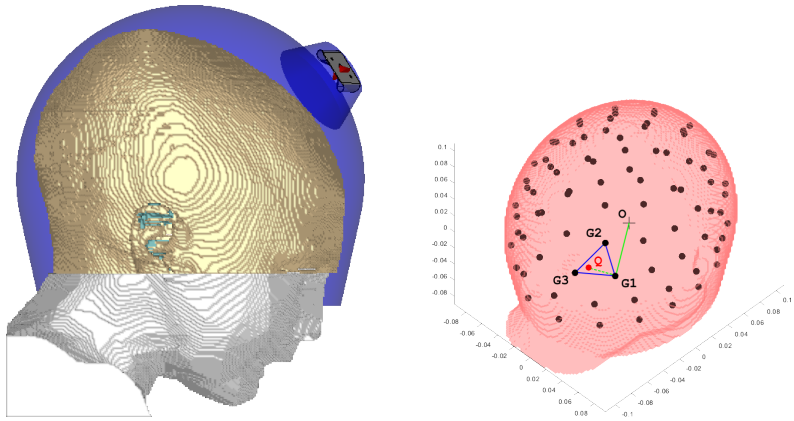

(a) Single Antenna Setup **(b)** Interpolation Grid

Figure 4.4: E-field interpolation method. A single antenna (a) is simulated at a number of fixed locations around the head (b). The E-field due to an antenna at query location Q is determine by linear weighed interpolation of the simulated E-fields at grid locations $G1$, $G2$ and $G3$.

In this study, the method was applied to the optimization of an illustrative case of applicator consisting of 8 antennas of the same size and a single-frequency treatment plan. The method was validated indirectly by comparing the improvement in APA (average power absorption, [102]) obtained by the optimized array versus a standard ring array to the improvement in APA indicated by a full FDTD simulation of the same two array configurations. The method was able to reflect the improvement in APA, which indicates that the optimization procedure based on the field approximation is effectively leading to a lower cost function value and better antenna arrangement for the specific patient.

In further, yet unpublished material, we have determined the actual approximation error by comparing the interpolated distribution with the fully simulated E-field of a single antenna at the same location and rotation. The errors due to varying location and rotation were assessed separately in two sweeps, Fig. 4.5. We provide a summary of the results in words:

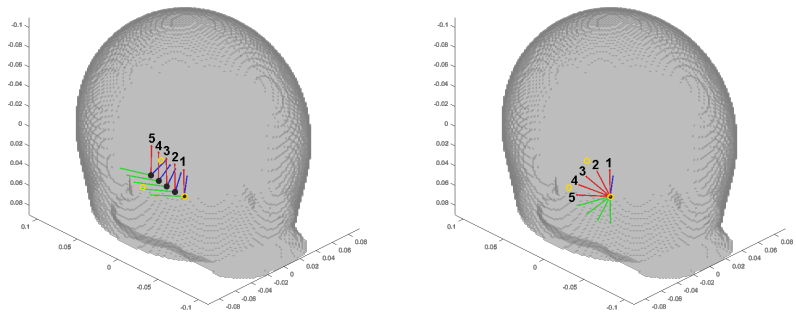

(a) Location Sweep **(b)** Rotation Sweep

Figure 4.5: The location and rotation sweeps used to assess the error of the interpolated E-field approximation. The antenna location is indicated by a black dot. The main polarization axis is indicated in red, and the radiation direction in blue. The yellow circles indicate the locations of the closest grid points forming the local triangular patch for interpolation. In (a), the antenna is moved in 5 steps from a simulated grid location towards the opposite edge via the center of the patch. In (b), the antenna is located at a grid point and its polarization is rotated in 5 steps between the two orthogonal simulated directions.

1. The approximation seems to be robust regardless of the operating frequency.
2. Location changes introduce an average error less than 3 % in phase and 10 % in radiation direction, while the amplitude error can reach as much as 37 % when the query location is far from the sampled grid locations.
3. The worst overall distribution error is around 26 %, which is acceptable for array optimization purposes.
4. The approximation of changes in the antenna's polarization angle is almost exact, with all errors lying below 5 % of the actual simulated distribution.

In conclusion, the results motivate the use of the proposed field interpolation technique for quick array evaluation and optimization.

4.2 Helmet array optimization: preliminary results

In this section, a preliminary investigation of the optimal helmet applicator configuration to treat a pediatric medulloblastoma patient is outlined, Fig. 4.6. Using the particle swarm global optimizer together with the fast UWB E-field approximation method and the fast i-TR UWB treatment planning algorithm described in the previous sections, we have obtained a first estimate of the HCQ-optimal array configuration consisting of 4 low-frequency

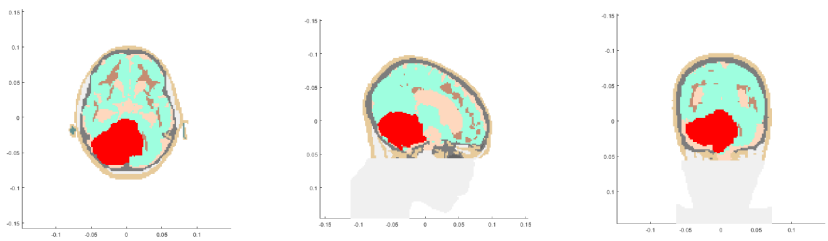

(a) Transverse **(b)** Sagittal **(c)** Coronal

Figure 4.6: Model of a pediatric patient showing a large medulloblastoma, highlighted in red. Sections taken at tumor center.

antennas (300 – 600 MHz) and 4 high-frequency antennas (400 – 800 MHz). The optimization was carried out for the [300, 400, 500, 600, 700, 800] MHz set of operating frequencies.

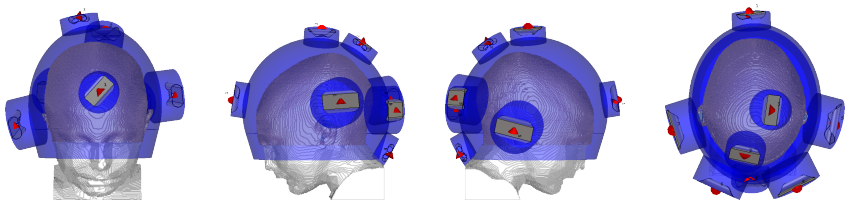

(a) Front **(b)** Left **(c)** Right **(d)** Top

Figure 4.7: Resulting helmet applicator antenna arrangement for the treatment of a large medulloblastoma in a pediatric patient. The array consists of 4 larger and 4 smaller antennas, operating at different and partially overlapping frequency bands.

Despite the large target volume, the final array arrangement, shown in Fig. 4.7, yields an HTQ value of 1.8 with quite an impressive TC_{25} at 83 %. In the subsequent thermal validation, Fig. 4.8, the achieved tumor temperatures are T_{90} = 38.6 °C and T_{50} = 39.7 °C while all healthy tissues are kept below a conservative temperature threshold of 42 °C. The limiting hot-spot emerges, as expected, in the cerebrospinal fluid adjacent to the brainstem. These encouraging results indicate that microwave heat delivery into large intracranial tumors is feasible and motivate the further development of specific applicators for this site.

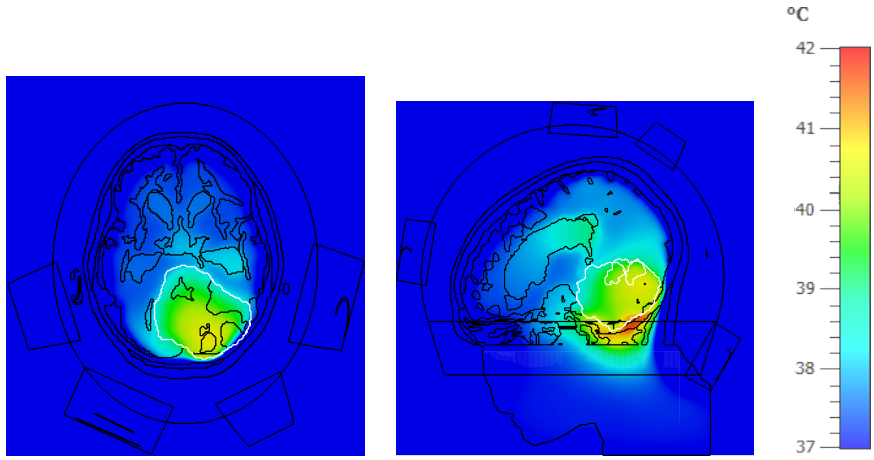

(a) Transverse **(b)** Sagittal

Figure 4.8: Temperature distribution obtained in the medulloblastoma patient using the optimized helmet applicator. The maximum temperature in all healthy tissues is 42 °C.

CHAPTER 5

Ongoing Work and Outlook

This thesis deals with different aspects of the development of UWB hyperthermia applicators to treat intracranial tumors. The results indicate that non-invasive UWB microwave hyperthermia is a viable treatment option in this location and that more research efforts should be spent in this direction. Patient-specific array design and treatment planning optimization can increase the tumor temperatures and the thermal dose to the levels required to achieve a therapeutic gain when combined with other treatment modalities. Nevertheless, from an engineering perspective, the task remains a challenge and has to be tackled from many angles. The development of a robust, reliable and safe microwave hyperthermia system is not limited to the design of a good applicator. A large number of practical issues has to been taken into account and solved before such a system can be adopted for clinical use.

First of all, the applicator has to be backed by a reliable RF amplifying system. Each channel in the RF cascade must be able to be steered in amplitude and phase at any frequency of the operating band within the necessary precision. The hyperthermia system and the clinical setup have to match the accuracy required for the treatment plan to be meaningfully applied [126]. The treatment plan optimization, in fact, assumes that the virtual model

corresponds exactly to the actual setup during a treatment sessions. Unfortunately, this is often not the case [127], as the patient and the applicator can be slightly misplaced with respect to each other. Furthermore, the currently used water-boli are prone to unpredictable shape deformations due to their thin plastic casings, and can also be subject to air leakages when the internal water pressure is insufficient. The presence of air bubbles and plastic layers between an antenna and the patient is detrimental for the treatment, as they cause unpredictable wave scattering and thus differences in the resulting power deposition pattern. A summary of possible mismatches is reported in Fig. 5.1.

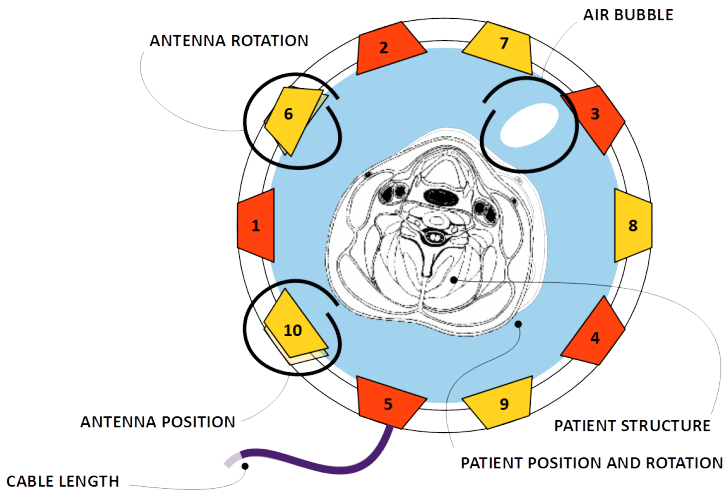

Figure 5.1: Potential mismatches between the assumptions made by the treatment planning optimizer and the actual treatment setup.

In parallel with a proper applicator design that can limit these uncertainties, we have initiated a study on the possibility to use a Vector Network Analyzer (VNA) in conjunction with the high power RF cascade to measure the scattering matrix of the applicator array, as illustrated in Fig. 5.2. The S-parameters are measured prior to treatment in the presence of the patient. The information contained in the S-matrix can then be processed to extract the unintended amount of phase delay and amplitude attenuation that each antenna is subject to during the particular treatment session [128]. These values are then subtracted from the treatment plan to compensate for mismatches between

the treatment planning and the clinical setup, thus implementing a form of self-calibration. The work is ongoing and experimental tests are needed to validate the applicability of this technique in real scenarios.

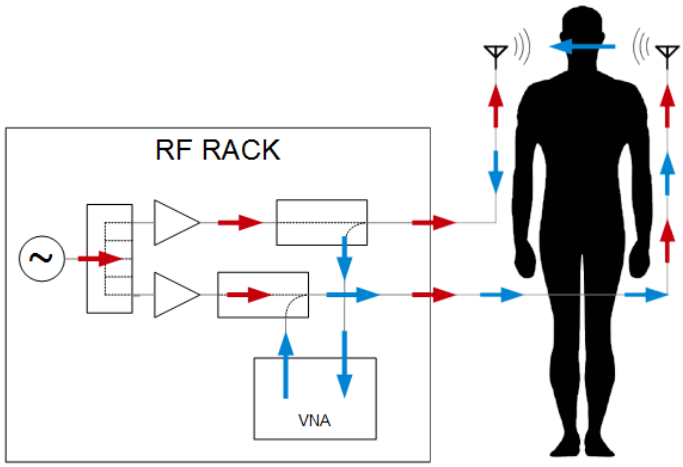

Figure 5.2: Integrating a VNA into a multi-channel UWB hyperthermia system has the potential to provide real-time feedback control of the power deposition inside the patient.

An additional benefit of integrating a VNA into a 16-channels UWB hyperthermia system is the possibility to perform real-time microwave tomography [129]. A combined imaging and treatment system could in fact allow for the measurement of the *in-vivo* dielectric properties of tissues prior to treatment and hopefully reduce the uncertainty in patient modelling that currently affects hyperthermia treatment plannings. The biomedical electromagnetics research group at Chalmers has a long-established experience in the field of theoretical and applied microwave image reconstruction [130]. Tomography measurements can also be performed repeatedly during treatment to track the variations in dielectric properties due to temperature changes. The technique can be used to non-invasively obtain a map of the actual temperature distribution inside the patient during treatment [131]–[133]. In other words, the integration of a VNA has the potential to "close the loop" in microwave hyperthermia treatments, providing the feedback control necessary for more accurate power delivery. Note that, in single-frequency systems, the informa-

tion acquired by this kind of measurement would be only limited and very likely not sufficient for this purpose. In an UWB system, information about the phase delay and amplitude attenuation can be obtained for the whole operating band, providing a much larger base for tomography computations. Work is ongoing to embed a low-cost and high dynamic range VNA for tomography measurements into Chalmers' hyperthermia system.

CHAPTER 6

Summary of included papers

This chapter provides a summary of the included papers.

6.1 Paper A

Massimiliano Zanoli, Hana Dobšíček Trefná
Suitability of eigenvalue beamforming for discrete multi-frequency hyperthermia treatment planning
Submitted to Medical Physics
24 December 2020

In this paper, we investigate whether using the eigenvalue (EV) decomposition to solve for the power deposition ratio Γ is a suitable method for single- and multi-frequency hyperthermia treatment planning optimization. We show that Γ cannot be maximized by more that one frequency at a time. In particular, even when the EV solver is complemented by an iterative optimization procedure that minimizes for another cost function, the final solution always consists of only one operating frequency, irrespective of how many frequencies are available for concomitant treatment. We further investigate whether the

single-frequency limitation represents a problem for deep microwave hyperthermia, and whether the use of multiple operating frequencies can improve target coverage and hot-spot suppression. Two realistic test cases are considered: a tumor in the larynx and a tumor in the meninges. We compare the resulting temperature distributions for a single frequency to the case when two simultaneous frequencies are jointly optimized with respect to their overall SAR distribution. The latter optimization is carried out using non-linear cost functions (HTQ and TC_{50}) and a global stochastic optimizer, Particle Swarm (PS). Results for the larynx indicate that a single frequency treatment may be sufficient to reach satisfying values of T_{50} and T_{90} in this region, as adding a secondary frequency does not improve the thermal distribution further. However, in the brain case, introducing a second frequency increases the SAR target coverage, TC_{50}, by 10 points, and temperature coverage, T_{90}, by 0.5 °C with respect to the best single-frequency solution (from 40.9 °C to 41.4 °C). In terms of $CEM_{43}T_{90}$, such an increase corresponds to a doubling of the thermal dose. We can conclude that multi-frequency systems do have the potential to substantially improve hyperthermia treatments in regions typically difficult to treat such as the brain.

6.2 Paper B

Massimiliano Zanoli, Hana Dobšíček Trefná
Combining target coverage and hot-spot suppression into one cost function: the hot-to-cold spot quotient
15th European Conference on Antennas and Propagation
22-26 March 2021, Düsseldorf, Germany

In this paper, we investigate the relationship between HTQ and TC_{50} and propose a novel cost-function for hyperthermia treatment planning optimization, the hot-to-cold spot quotient (HCQ). The HCQ is intended to combine the well known SAR metrics into one, thus enabling the concomitant optimization of both. We consider two realistic test cases, a target located in the larynx and one in the meningioma. A global stochastic optimizer is used to obtain the optimal treatment plans with respect to all three indicators. The results suggest that HTQ and TC_{50} assess different and not necessarily correlated aspects of a hyperthermia treatment plan. In particular, optimizing for the HTQ often yields too low values of TC_{50} for the treatment to be viable.

An analogous issue occurs when optimizing for TC_{50}: the resulting HTQ is systematically high, indicating that the most prominent hot-spot might be limiting for the treatment. When HCQ is used as cost function, the treatment planning optimization yields solutions exhibiting both low HTQ and high TC_{50}. Moreover, the HCQ works consistently in both single- and multi-frequency settings. Given a discrete set of possible operating frequencies, the HCQ-based optimizer can always determine a combination of one or more frequencies that exhibit HCQ and TC_{50} close to their globally optimal values in the examined cases. Furthermore, the proposed definition of HCQ guarantees that this value is always normalized to the patient and target volume, rendering values of HCQ from different plans comparable. It can be concluded that HCQ provides the means for an effective multi-frequency HTP optimization and enables meaningful comparisons between large numbers of potential solutions. Future work will include a thermal validation of the HCQ-temperature relationship on clinical data sets.

6.3 Paper C

Massimiliano Zanoli, Hana Dobšíček Trefná
Iterative time-reversal for multi-frequency hyperthermia
Physics in Medicine & Biology
16 December 2020

DOI: 10.1088/1361-6560/abd41a

In this paper, we propose a novel, deterministic UWB iterative scheme based on time-reversal (i-TR). The method, which aims at minimizing the hot-to-cold spot quotient (HCQ), improves hot-spot suppression and target coverage of classic time-reversal (TR) based microwave hyperthermia treatment planning. The procedure is initialized at the TR solution obtained by placing a virtual source at the center of the tumor mass. The resulting, time reversed, SAR distribution is analysed and the most prominent cold-spot and hot-spot are identified in the tumor and in the healthy tissues, respectively. Two TR solutions are then determined at the cold- and hot-spot centers. The algorithm improves the current solution by progressively shifting the steering phases towards the cold-spot solution and the steering amplitudes away from the cold-spot solution. The procedure is reiterated and the algorithm halts

when the HCQ no longer improves. In this study, we show that i-TR yields results comparable to those obtained via global stochastic optimization, while being significantly faster. The algorithm is benchmarked numerically for two different applicator array topologies: a collar for tumors in the neck and a helmet for intracranial tumors. For the neck model, different target locations and sizes are considered, to assess the algorithm's robustness to different scenarios. The algorithm is also applied to two realistic cases: a tumor in the larynx and one in the meninges. For each test case, HTP quality and performance indicators are computed and compared against those obtained with eigenvalue, particle swarm and classic TR. The results suggest that the method is successful in finding viable multi-frequency solutions for a given problem, independently of the target's size, location, morphology or composition. They further indicate that the method is robust to problems involving mixed polarization axes. The treatment plans obtained via i-TR are further validated with thermal simulations. It is shown that i-TR can achieve similar tumor temperatures (T_{50}) as the treatment plans based on global HTQ optimization. In the larynx case, i-TR outperforms the HTQ-based plan by 0.4 °C, advocating the suitability of the HCQ as cost function for optimization.

6.4 Paper D

Massimiliano Zanoli, Hana Dobšíček Trefná
Optimization of microwave hyperthermia array applicators using field interpolation
2019 IEEE International Symposium on Antennas and Propagation and USNC-URSI Radio Science Meeting
537–538, 7-12 July 2019, Atlanta, USA

In this paper, we present a novel field interpolation technique that allows for the quick estimation of the E-field distributions generated by a particular array arrangement at any operating frequency. The interpolation is based on a pre-calculated set of E-field distributions generated by a single antenna placed at fixed locations around the head (interpolation grid). For each location, two orthogonal polarization directions are simulated. The E-field generated by an antenna at a specific location and rotation is then obtained by a weighed average of the three nearest sampled locations. The method is applied to the optimization of an illustrative case of an applicator consisting of 8 antennas of

the same size and a single-frequency treatment plan. The method is validated indirectly by comparing the improvement in average power absorption ratio (APA) obtained by the optimized array versus a standard ring array to the improvement in APA indicated by a full simulation of the same two array configurations. The method is shown to reflect the improvement in APA, indicating that the optimization procedure based on the field approximation is effectively leading to a better cost function value and better antenna arrangement for the specific case assessed in this study.

References

[1] Global Burden of Disease Collaborative Network, "Global Burden of Disease Study 2017 (GBD 2017)", *Institute for Health Metrics and Evaluation (IHME)*, 2018.

[2] C. P. Wild, E. Weiderpass, and B. W. Stewart, *World cancer report: Cancer research for cancer prevention*, Feb. 2020.

[3] American Cancer Society, *Cancer Facts & Figures 2020*, Atlanta, US, 2020.

[4] N. H. S. (NHS), *Malignant brain tumour (brain cancer)*, Mar. 2018.

[5] I. F. Pollack, S. Agnihotri, and A. Broniscer, "Childhood brain tumors: Current management, biological insights, and future directions: Jnspg 75th anniversary invited review article", *Journal of Neurosurgery: Pediatrics*, vol. 23, no. 3, pp. 261–273, 2019.

[6] E. Livesey and C. Brook, "Gonadal dysfunction after treatment of intracranial tumours.", *Archives of disease in childhood*, vol. 63, no. 5, pp. 495–500, 1988.

[7] B. Lannering, I. Marky, A. Lundberg, and E. Olsson, "Long-term sequelae after pediatric brain tumors: Their effect on disability and quality of life", *Medical and pediatric oncology*, vol. 18, no. 4, pp. 304–310, 1990.

[8] E. Nicklin, G. Velikova, C. Hulme, R. Rodriguez Lopez, A. Glaser, M. Kwok-Williams, and F. Boele, "Long-term issues and supportive care needs of adolescent and young adult childhood brain tumour survivors and their caregivers: A systematic review", *Psycho-oncology*, vol. 28, no. 3, pp. 477–487, 2019.

[9] S. Roussakow, "The history of hyperthermia rise and decline", in *Conference Papers in Science*, Hindawi, vol. 2013, 2013.

[10] N. Cihoric, A. Tsikkinis, G. van Rhoon, H. Crezee, D. M. Aebersold, S. Bodis, M. Beck, J. Nadobny, V. Budach, P. Wust, *et al.*, "Hyperthermia-related clinical trials on cancer treatment within the clinicaltrials. gov registry", *International journal of hyperthermia*, vol. 31, no. 6, pp. 609–614, 2015.

[11] N. R. Datta, S. Rogers, S. G. Ordóñez, E. Puric, and S. Bodis, "Hyperthermia and radiotherapy in the management of head and neck cancers: A systematic review and meta-analysis", *International Journal of Hyperthermia*, vol. 32, no. 1, pp. 31–40, 2016.

[12] N. R. Datta, E. Puric, D. Klingbiel, S. Gomez, and S. Bodis, "Hyperthermia and radiation therapy in locoregional recurrent breast cancers: A systematic review and meta-analysis", *International Journal of Radiation Oncology* Biology* Physics*, vol. 94, no. 5, pp. 1073–1087, 2016.

[13] N. R. Datta, E. Stutz, S. Gomez, and S. Bodis, "Efficacy and safety evaluation of the various therapeutic options in locally advanced cervix cancer: A systematic review and network meta-analysis of randomized clinical trials", *International Journal of Radiation Oncology* Biology* Physics*, vol. 103, no. 2, pp. 411–437, 2019.

[14] M. Paulides, H. D. Trefná, S. Curto, and D. Rodrigues, "Recent technological advancements in radiofrequency-and microwave-mediated hyperthermia for enhancing drug delivery.", *Advanced Drug Delivery Reviews*, 2020.

[15] M. Franckena, L. J. Stalpers, P. C. Koper, R. G. Wiggenraad, W. J. Hoogenraad, J. D. van Dijk, C. C. Wárlám-Rodenhuis, J. J. Jobsen, G. C. van Rhoon, and J. van der Zee, "Long-term improvement in treatment outcome after radiotherapy and hyperthermia in locoregionally advanced cervix cancer: An update of the dutch deep hyperthermia

trial", *International Journal of Radiation Oncology* Biology* Physics*, vol. 70, no. 4, pp. 1176–1182, 2008.

[16] R. D. Issels, L. H. Lindner, J. Verweij, R. Wessalowski, P. Reichardt, P. Wust, P. Ghadjar, P. Hohenberger, M. Angele, C. Salat, *et al.*, "Effect of neoadjuvant chemotherapy plus regional hyperthermia on long-term outcomes among patients with localized high-risk soft tissue sarcoma: The eortc 62961-esho 95 randomized clinical trial", *JAMA oncology*, vol. 4, no. 4, pp. 483–492, 2018.

[17] A. Winter, J. Laing, R. Paglione, and F. Sterzer, "Microwave hyperthermia for brain tumors", *Neurosurgery*, vol. 17, no. 3, pp. 387–399, 1985.

[18] R. Tanaka, C. H. Kim, N. Yamada, and Y. Saito, "Radiofrequency hyperthermia for malignant brain tumors: Preliminary results of clinical trials", *Neurosurgery*, vol. 21, no. 4, pp. 1–3, 1987.

[19] P. K. Sneed, P. H. Gutin, P. R. Stauffer, T. L. Phillips, M. D. Prados, K. A. Weaver, S. Suen, S. A. Lamb, B. Ham, D. K. Ahn, *et al.*, "Thermoradiotherapy of recurrent malignant brain tumors", *International Journal of Radiation Oncology* Biology* Physics*, vol. 23, no. 4, pp. 853–861, 1992.

[20] P. Gas, "Essential facts on the history of hyperthermia and their connections with electromedicine", *arXiv preprint arXiv:1710.00652*, 2017.

[21] S. S. Evans, E. A. Repasky, and D. T. Fisher, "Fever and the thermal regulation of immunity: The immune system feels the heat", *Nature Reviews Immunology*, vol. 15, no. 6, pp. 335–349, 2015.

[22] N. van den Tempel, M. R. Horsman, and R. Kanaar, "Improving efficacy of hyperthermia in oncology by exploiting biological mechanisms", *International journal of hyperthermia*, vol. 32, no. 4, pp. 446–454, 2016.

[23] M. W. Dewhirst, C.-T. Lee, and K. A. Ashcraft, "The future of biology in driving the field of hyperthermia", *International Journal of Hyperthermia*, vol. 32, no. 1, pp. 4–13, 2016.

[24] K. F. Chu and D. E. Dupuy, "Thermal ablation of tumours: Biological mechanisms and advances in therapy", *Nature Reviews Cancer*, vol. 14, no. 3, pp. 199–208, 2014.

[25] P. R. Stauffer and M. M. Paulides, "Hyperthermia therapy for cancer", *Comprehensive biomedical physics*, vol. 10, no. 07, pp. 115–151, 2014.

[26] H. H. Kampinga, "Cell biological effects of hyperthermia alone or combined with radiation or drugs: A short introduction to newcomers in the field", *International journal of hyperthermia*, vol. 22, no. 3, pp. 191–196, 2006.

[27] R. Issels, E. Kampmann, R. Kanaar, and L. H. Lindner, "Hallmarks of hyperthermia in driving the future of clinical hyperthermia as targeted therapy: Translation into clinical application", *International Journal of Hyperthermia*, vol. 32, no. 1, pp. 89–95, 2016.

[28] A. Oei, H. Kok, S. Oei, M. Horsman, L. Stalpers, N. Franken, and J. Crezee, "Molecular and biological rationale of hyperthermia as radio- and chemosensitizer", *Advanced drug delivery reviews*, 2020.

[29] M. R. Horsman and J. Overgaard, "Hyperthermia: A potent enhancer of radiotherapy", *Clinical oncology*, vol. 19, no. 6, pp. 418–426, 2007.

[30] M. W. Dewhirst, Z. Vujaskovic, E. Jones, and D. Thrall, "Re-setting the biologic rationale for thermal therapy", *International Journal of Hyperthermia*, vol. 21, no. 8, pp. 779–790, 2005.

[31] J. C. Peeken, P. Vaupel, and S. E. Combs, "Integrating hyperthermia into modern radiation oncology: What evidence is necessary?", *Frontiers in oncology*, vol. 7, p. 132, 2017.

[32] G. C. Van Rhoon and P. Wust, "Introduction: Non-invasive thermometry for thermotherapy", *International Journal of Hyperthermia*, vol. 21, no. 6, pp. 489–495, 2005.

[33] H. P. Kok, E. N. Cressman, W. Ceelen, C. L. Brace, R. Ivkov, H. Grüll, G. Ter Haar, P. Wust, and J. Crezee, "Heating technology for malignant tumors: A review", *International Journal of Hyperthermia*, vol. 37, no. 1, pp. 711–741, 2020.

[34] G. P. Skandalakis, D. R. Rivera, C. D. Rizea, A. Bouras, J. G. Jesu Raj, D. Bozec, and C. G. Hadjipanayis, "Hyperthermia treatment advances for brain tumors", *International Journal of Hyperthermia*, vol. 37, no. 2, pp. 3–19, 2020.

[35] M. Salcman and G. M. Samaras, "Interstitial microwave hyperthermia for brain tumors", *Journal of Neuro-oncology*, vol. 1, no. 3, pp. 225–236, 1983.

[36] P. K. Sneed, P. R. Stauffer, M. W. McDermott, C. J. Diederich, K. R. Lamborn, M. D. Prados, S. Chang, K. A. Weaver, L. Spry, M. K. Malec, *et al.*, "Survival benefit of hyperthermia in a prospective randomized trial of brachytherapy boost+hyperthermia for glioblastoma multiforme", *International Journal of Radiation Oncology* Biology* Physics*, vol. 40, no. 2, pp. 287–295, 1998.

[37] M. Wankhede, A. Bouras, M. Kaluzova, and C. G. Hadjipanayis, "Magnetic nanoparticles: An emerging technology for malignant brain tumor imaging and therapy", *Expert review of clinical pharmacology*, vol. 5, no. 2, pp. 173–186, 2012.

[38] R. Stupp, M. E. Hegi, W. P. Mason, M. J. Van Den Bent, M. J. Taphoorn, R. C. Janzer, S. K. Ludwin, A. Allgeier, B. Fisher, K. Belanger, *et al.*, "Effects of radiotherapy with concomitant and adjuvant temozolomide versus radiotherapy alone on survival in glioblastoma in a randomised phase iii study: 5-year analysis of the eortc-ncic trial", *The lancet oncology*, vol. 10, no. 5, pp. 459–466, 2009.

[39] K. Maier-Hauff, F. Ulrich, D. Nestler, H. Niehoff, P. Wust, B. Thiesen, H. Orawa, V. Budach, and A. Jordan, "Efficacy and safety of intratumoral thermotherapy using magnetic iron-oxide nanoparticles combined with external beam radiotherapy on patients with recurrent glioblastoma multiforme", *Journal of neuro-oncology*, vol. 103, no. 2, pp. 317–324, 2011.

[40] Z. Ram, Z. R. Cohen, S. Harnof, S. Tal, M. Faibel, D. Nass, S. E. Maier, M. Hadani, and Y. Mardor, "Magnetic resonance imaging-guided, high-intensity focused ultrasound forbrain tumortherapy", *Neurosurgery*, vol. 59, no. 5, pp. 949–956, 2006.

[41] F. Prada, M. Y. S. Kalani, K. Yagmurlu, P. Norat, M. Del Bene, F. DiMeco, and N. F. Kassell, "Applications of focused ultrasound in cerebrovascular diseases and brain tumors", *Neurotherapeutics*, vol. 16, no. 1, pp. 67–87, 2019.

[42] G. Schooneveldt, H. D. Trefná, M. Persson, T. M. De Reijke, K. Blomgren, H. P. Kok, and H. Crezee, "Hyperthermia treatment planning including convective flow in cerebrospinal fluid for brain tumour hyperthermia treatment using a novel dedicated paediatric brain applicator", *Cancers*, vol. 11, no. 8, p. 1183, 2019.

[43] M. Paulides, J. Bakker, E. Neufeld, J. v. d. Zee, P. Jansen, P. Levendag, and G. Van Rhoon, "The HYPERcollar: A novel applicator for hyperthermia in the head and neck", *International Journal of Hyperthermia*, vol. 23, no. 7, pp. 567–576, 2007.

[44] P. Wust, H. Fähling, T. Helzel, M. Kniephoff, W. Wlodarczyk, G. Mönich, and R. Felix, "Design and test of a new multi-amplifier system with phase and amplitude control", *International journal of hyperthermia*, vol. 14, no. 5, pp. 459–477, 1998.

[45] J. Crezee, P. Van Haaren, H. Westendorp, M. De Greef, H. Kok, J. Wiersma, G. Van Stam, J. Sijbrands, P. Zum Vörde Sive Vörding, J. Van Dijk, *et al.*, "Improving locoregional hyperthermia delivery using the 3-d controlled amc-8 phased array hyperthermia system: A preclinical study", *International Journal of Hyperthermia*, vol. 25, no. 7, pp. 581–592, 2009.

[46] R. Zweije, H. P. Kok, A. Bakker, A. Bel, and J. Crezee, "Technical and clinical evaluation of the ALBA-4D 70mhz loco-regional hyperthermia system", in *2018 48th European Microwave Conference (EuMC)*, IEEE, 2018, pp. 328–331.

[47] M. Paulides, Z. Rijnen, P. Togni, R. Verhaart, T. Drizdal, D. De Jong, M. Franckena, G. Verduijn, and G. Van Rhoon, "Clinical introduction of novel microwave hyperthermia technology: The hypercollar3d applicator for head and neck hyperthermia", in *2015 9th European Conference on Antennas and Propagation (EuCAP)*, IEEE, 2015, pp. 1–4.

[48] M. Converse, E. J. Bond, B. Veen, and C. Hagness, "A computational study of ultra-wideband versus narrowband microwave hyperthermia for breast cancer treatment", *IEEE transactions on microwave theory and techniques*, vol. 54, no. 5, pp. 2169–2180, 2006.

[49] H. D. Trefná, J. Vrba, and M. Persson, "Evaluation of a patch antenna applicator for time reversal hyperthemia", *International Journal of Hyperthermia*, vol. 26, no. 2, pp. 185–197, 2010.

[50] G. G. Bellizzi, L. Crocco, G. M. Battaglia, and T. Isernia, "Multi-frequency constrained SAR focusing for patient specific hyperthermia treatment", *IEEE Journal of Electromagnetics, RF and Microwaves in Medicine and Biology*, vol. 1, no. 2, pp. 74–80, 2017.

[51] L. Winter, C. Oezerdem, W. Hoffmann, T. van de Lindt, J. Periquito, Y. Ji, P. Ghadjar, V. Budach, P. Wust, and T. Niendorf, "Thermal magnetic resonance: Physics considerations and electromagnetic field simulations up to 23.5 tesla (1ghz)", *Radiation Oncology*, vol. 10, no. 1, pp. 1–12, 2015.

[52] P. Takook, M. Persson, and H. D. Trefná, "Performance evaluation of hyperthermia applicators to heat deep-seated brain tumors", *IEEE Journal of Electromagnetics, RF and Microwaves in Medicine and Biology*, vol. 2, no. 1, pp. 18–24, 2018.

[53] A. Kuehne, E. Oberacker, H. Waiczies, and T. Niendorf, "Solving the time-and frequency-multiplexed problem of constrained radiofrequency induced hyperthermia", *Cancers*, vol. 12, no. 5, p. 1072, 2020.

[54] P. S. Yarmolenko, E. J. Moon, C. Landon, A. Manzoor, D. W. Hochman, B. L. Viglianti, and M. W. Dewhirst, "Thresholds for thermal damage to normal tissues: An update", *International Journal of Hyperthermia*, vol. 27, no. 4, pp. 320–343, 2011.

[55] S. Gavazzi, A. L. van Lier, C. Zachiu, E. Jansen, J. J. W. Lagendijk, L. J. A. Stalpers, H. Crezee, and H. P. Kok, "Advanced patient-specific hyperthermia treatment planning", *International Journal of Hyperthermia*, vol. 37, no. 1, pp. 992–1007, 2020.

[56] P. F. Turner, "Regional hyperthermia with an annular phased array", *IEEE Transactions on Biomedical Engineering*, no. 1, pp. 106–114, 1984.

[57] H. P. Kok, L. Korshuize-van Straten, A. Bakker, R. de Kroon-Oldenhof, E. D. Geijsen, L. J. Stalpers, and J. Crezee, "Online adaptive hyperthermia treatment planning during locoregional heating to suppress treatment-limiting hot spots", *International Journal of Radiation Oncology* Biology* Physics*, vol. 99, no. 4, pp. 1039–1047, 2017.

[58] H. D. Trefná, B. Martinsson, T. Petersson, N. Renström, M. Torstensson, J. Ravanis, P. Kok, and M. Persson, "Multifrequency approach in hyperthermia treatment planning: Impact of frequency on sar distribution in head and neck", in *2017 11th European Conference on Antennas and Propagation (EUCAP)*, IEEE, 2017, pp. 3710–3712.

[59] M. M. Paulides, P. R. Stauffer, E. Neufeld, P. F. Maccarini, A. Kyriakou, R. A. Canters, C. J. Diederich, J. F. Bakker, and G. C. Van Rhoon, "Simulation techniques in hyperthermia treatment planning", *International Journal of Hyperthermia*, vol. 29, no. 4, pp. 346–357, 2013.

[60] P. Hasgall, F. Di Gennaro, C. Baumgartner, E. Neufeld, B. Lloyd, M. Gosselin, D. Payne, A. Klingenböck, and N. Kuster, *IT'IS Database for thermal and electromagnetic parameters of biological tissues*, version 4.0, May 2018.

[61] A. M. Stoll and L. C. Greene, "Relationship between pain and tissue damage due to thermal radiation", *Journal of applied physiology*, vol. 14, no. 3, pp. 373–382, 1959.

[62] H. Kok, P. Wust, P. R. Stauffer, F. Bardati, G. Van Rhoon, and J. Crezee, "Current state of the art of regional hyperthermia treatment planning: A review", *Radiation Oncology*, vol. 10, no. 1, p. 196, 2015.

[63] R. Canters, P. Wust, J. Bakker, and G. Van Rhoon, "A literature survey on indicators for characterisation and optimisation of sar distributions in deep hyperthermia, a plea for standardisation", *International Journal of Hyperthermia*, vol. 25, no. 7, pp. 593–608, 2009.

[64] H. P. Kok, J. Gellermann, C. A. van den Berg, P. R. Stauffer, J. W. Hand, and J. Crezee, "Thermal modelling using discrete vasculature for thermal therapy: A review", *International Journal of Hyperthermia*, vol. 29, no. 4, pp. 336–345, 2013.

[65] M. De Greef, H. Kok, D. Correia, A. Bel, and J. Crezee, "Optimization in hyperthermia treatment planning: The impact of tissue perfusion uncertainty", *Medical physics*, vol. 37, no. 9, pp. 4540–4550, 2010.

[66] R. A. Canters, M. M. Paulides, M. F. Franckena, J. van der Zee, and G. C. van Rhoon, "Implementation of treatment planning in the routine clinical procedure of regional hyperthermia treatment of cervical cancer: An overview and the Rotterdam experience", *International journal of hyperthermia*, vol. 28, no. 6, pp. 570–581, 2012.

[67] R. Canters, M. Paulides, M. Franckena, J. Mens, and G. Van Rhoon, "Benefit of replacing the sigma-60 by the sigma-eye applicator", *Strahlentherapie und Onkologie*, vol. 189, no. 1, pp. 74–80, 2013.

[68] Z. Rijnen, J. F. Bakker, R. A. Canters, P. Togni, G. M. Verduijn, P. C. Levendag, G. C. Van Rhoon, and M. M. Paulides, "Clinical integration of software tool vedo for adaptive and quantitative application of phased array hyperthermia in the head and neck", *International journal of Hyperthermia*, vol. 29, no. 3, pp. 181–193, 2013.

[69] R. F. Verhaart, V. Fortunati, G. M. Verduijn, A. van der Lugt, T. van Walsum, J. F. Veenland, and M. M. Paulides, "The relevance of mri for patient modeling in head and neck hyperthermia treatment planning: A comparison of ct and ct-mri based tissue segmentation on simulated temperature", *Medical physics*, vol. 41, no. 12, p. 123 302, 2014.

[70] I. VilasBoas-Ribeiro, G. C. van Rhoon, T. Drizdal, M. Franckena, and M. M. Paulides, "Impact of number of segmented tissues on sar prediction accuracy in deep pelvic hyperthermia treatment planning", *Cancers*, vol. 12, no. 9, p. 2646, 2020.

[71] G. G. Bellizzi, T. Drizdal, G. C. van Rhoon, L. Crocco, T. Isernia, and M. M. Paulides, "The potential of constrained sar focusing for hyperthermia treatment planning: Analysis for the head & neck region", *Physics in Medicine & Biology*, vol. 64, no. 1, p. 015 013, 2018.

[72] N. Lynnerup, "Cranial thickness in relation to age, sex and general body build in a danish forensic sample", *Forensic science international*, vol. 117, no. 1-2, pp. 45–51, 2001.

[73] A. Peyman, "Dielectric properties of tissues; variation with age and their relevance in exposure of children to electromagnetic fields; state of knowledge", *Progress in biophysics and molecular biology*, vol. 107, no. 3, pp. 434–438, 2011.

[74] D. A. Pollacco, L. Farina, P. S. Wismayer, L. Farrugia, and C. V. Sammut, "Characterization of the dielectric properties of biological tissues and their correlation to tissue hydration", *IEEE Transactions on Dielectrics and Electrical Insulation*, vol. 25, no. 6, pp. 2191–2197, 2018.

[75] C. W. Song, "Effect of local hyperthermia on blood flow and microenvironment: A review", *Cancer research*, vol. 44, no. 10 Supplement, 4721s–4730s, 1984.

[76] C. Rossmann and D. Haemmerich, "Review of temperature dependence of thermal properties, dielectric properties, and perfusion of biological tissues at hyperthermic and ablation temperatures", *Critical Reviews^{TM} in Biomedical Engineering*, vol. 42, no. 6, 2014.

[77] M. M. Paulides, D. B. Rodrigues, G. G. Bellizzi, K. Sumser, S. Curto, E. Neufeld, H. P. Kok, and H. D. Trefná, "Esho benchmarks for computational modeling and optimization in hyperthermia therapy", *submitted to International Journal of Hyperthermia*, 2021.

[78] J. Van de Kamer, N. Van Wieringen, A. De Leeuw, and J. Lagendijk, "The significance of accurate dielectric tissue data for hyperthermia treatment planning", *International journal of hyperthermia*, vol. 17, no. 2, pp. 123–142, 2001.

[79] J. Lang, B. Erdmann, and M. Seebass, "Impact of nonlinear heat transfer on temperature control in regional hyperthermia", *IEEE Transactions on Biomedical Engineering*, vol. 46, no. 9, pp. 1129–1138, 1999.

[80] J.-P. Berenger, "A perfectly matched layer for the absorption of electromagnetic waves", *Journal of computational physics*, vol. 114, no. 2, pp. 185–200, 1994.

[81] H. H. Pennes, "Analysis of tissue and arterial blood temperatures in the resting human forearm", *Journal of applied physiology*, vol. 1, no. 2, pp. 93–122, 1948.

[82] Dassault Systèmes SE, Vélizy-Villacoublay, France, *CST Studio Suite 2019*, 2019.

[83] W. C. Dewey, "Arrhenius relationships from the molecule and cell to the clinic", *International journal of hyperthermia*, vol. 10, no. 4, pp. 457–483, 1994.

[84] E. L. Jones, J. R. Oleson, L. R. Prosnitz, T. V. Samulski, Z. Vujaskovic, D. Yu, L. L. Sanders, M. W. Dewhirst, *et al.*, "Randomized trial of hyperthermia and radiation for superficial tumors", *Journal of Clinical Oncology*, vol. 23, no. 13, pp. 3079–3085, 2005.

[85] G. C. van Rhoon, "Is CEM43 still a relevant thermal dose parameter for hyperthermia treatment monitoring?", *International Journal of Hyperthermia*, vol. 32, no. 1, pp. 50–62, 2016.

[86] M. M. Paulides, G. M. Verduijn, and N. Van Holthe, "Status quo and directions in deep head and neck hyperthermia", *Radiation Oncology*, vol. 11, no. 1, p. 21, 2016.

[87] G. G. Bellizzi, T. Drizdal, G. C. van Rhoon, L. Crocco, T. Isernia, and M. M. Paulides, "Predictive value of sar based quality indicators for head and neck hyperthermia treatment quality", *International Journal of Hyperthermia*, vol. 36, no. 1, pp. 455–464, 2019.

[88] R. Canters, M. Franckena, J. van der Zee, and G. Van Rhoon, "Optimizing deep hyperthermia treatments: Are locations of patient pain complaints correlated with modelled SAR peak locations?", *Physics in Medicine & Biology*, vol. 56, no. 2, p. 439, 2010.

[89] H. K. Lee, A. G. Antell, C. A. Perez, W. L. Straube, G. Ramachandran, R. J. Myerson, B. Emami, E. P. Molmenti, A. Buckner, and M. A. Lockett, "Superficial hyperthermia and irradiation for recurrent breast carcinoma of the chest wall: Prognostic factors in 196 tumors.", *International journal of radiation oncology, biology, physics*, vol. 40, no. 2, pp. 365–375, 1998.

[90] I. E. C. (IEC), "Measurement procedure for the assessment of specific absorption rate of human exposure to radio frequency fields from hand-held and body-worn wireless communication devices - part 1528: Human models, instrumentation and procedures (frequency range of 4 mhz to 10 ghz)", 3, rue de Varembé, PO Box 131, CH-1211 Geneva 20, Switzerland, International Standard 62209-1528:2020, Oct. 2020.

[91] N. Stevens and L. Martens, "Study on the mass averaging of sar distributions", in *1999 IEEE MTT-S International Microwave Symposium Digest (Cat. No. 99CH36282)*, IEEE, vol. 2, 1999, pp. 595–598.

[92] A. Hirata, K. Shirai, and O. Fujiwara, "On averaging mass of sar correlating with temperature elevation due to a dipole antenna", *Progress In Electromagnetics Research*, vol. 84, pp. 221–237, 2008.

[93] A. Razmadze, L. Shoshiashvili, D. Kakulia, and R. Zaridze, "Influence on averaging masses on correlation between mass-averaged sar and temperature rise", *Journal of Applied Electromagnetism*, vol. 10, no. 2, pp. 8–21, 2008.

[94] A. Razmadze, L. Shoshiashvili, D. Kakulia, R. Zaridze, G. Bit-Babik, and A. Faraone, "Influence of specific absorption rate averaging schemes on correlation between mass-averaged specific absorption rate and temperature rise", *Electromagnetics*, vol. 29, no. 1, pp. 77–90, 2009.

[95] J. Bakker, M. Paulides, E. Neufeld, A. Christ, N. Kuster, and G. Van Rhoon, "Children and adults exposed to electromagnetic fields at the icnirp reference levels: Theoretical assessment of the induced peak temperature increase", *Physics in Medicine & Biology*, vol. 56, no. 15, p. 4967, 2011.

[96] K. Chopra, D. Calva, M. Sosin, K. K. Tadisina, A. Banda, C. De La Cruz, M. R. Chaudhry, T. Legesse, C. B. Drachenberg, P. N. Manson, *et al.*, "A comprehensive examination of topographic thickness of skin in the human face", *Aesthetic surgery journal*, vol. 35, no. 8, pp. 1007–1013, 2015.

[97] F. B. Haeussinger, S. Heinzel, T. Hahn, M. Schecklmann, A.-C. Ehlis, and A. J. Fallgatter, "Simulation of near-infrared light absorption considering individual head and prefrontal cortex anatomy: Implications for optical neuroimaging", *PloS one*, vol. 6, no. 10, e26377, 2011.

[98] N. Qi, M. Zhang, T. Wittig, and A. Prokop, "Application of CST time domain algorithm in the electromagnetic simulation standard of the SAR for mobile phone", in *2008 International Conference on Microwave and Millimeter Wave Technology*, IEEE, vol. 4, 2008, pp. 1717–1720.

[99] M. Böhm, J. Kremer, and A. Louis, "Efficient algorithm for computing optimal control of antennas in hyperthermia", *Surveys Math. Indust*, vol. 3, no. 4, pp. 233–251, 1993.

[100] T. Köhler, P. Maass, P. Wust, and M. Seebass, "A fast algorithm to find optimal controls of multiantenna applicators in regional hyperthermia", *Physics in Medicine & Biology*, vol. 46, no. 9, p. 2503, 2001.

[101] R. Mestrom, J. Van Engelen, M. Van Beurden, M. Paulides, W. Numan, and A. Tijhuis, "A refined eigenvalue-based optimization technique for hyperthermia treatment planning", in *The 8th European Conference on Antennas and Propagation (EuCAP 2014)*, IEEE, 2014, pp. 2010–2013.

[102] M. M. Paulides, S. H. Vossen, A. P. Zwamborn, and G. C. van Rhoon, "Theoretical investigation into the feasibility to deposit rf energy centrally in the head-and-neck region", *International Journal of Radiation Oncology* Biology* Physics*, vol. 63, no. 2, pp. 634–642, 2005.

[103] F. Bardati and P. Tognolatti, "Hyperthermia phased arrays pre-treatment evaluation", *International Journal of Hyperthermia*, vol. 32, no. 8, pp. 911–922, 2016.

[104] B. Guérin, J. F. Villena, A. G. Polimeridis, E. Adalsteinsson, L. Daniel, J. K. White, B. R. Rosen, and L. L. Wald, "Computation of ultimate SAR amplification factors for radiofrequency hyperthermia in non-uniform body models: Impact of frequency and tumour location", *International Journal of Hyperthermia*, vol. 34, no. 1, pp. 87–100, 2018.

[105] M. Zanoli and H. D. Trefná, "Suitability of eigenvalue beamforming for discrete multi-frequency hyperthermia treatment planning", *Medical Physics*, 2021, Manuscript submitted for publication.

[106] ——, "Combining target coverage and hot-spot suppression into one cost function: The hot-to-cold spot quotient", in *15th European Conference on Antennas and Propagation*, EurAAP, Mar. 2021, Accepted for publication.

[107] J. Kennedy and R. Eberhart, "Particle swarm optimization", in *Proceedings of ICNN'95-international conference on neural networks*, IEEE, vol. 4, 1995, pp. 1942–1948.

[108] G. Cappiello, T. Drizdal, B. Mc Ginley, M. O'Halloran, M. Glavin, G. Van Rhoon, E. Jones, and M. Paulides, "The potential of time-multiplexed steering in phased array microwave hyperthermia for head and neck cancer treatment", *Physics in Medicine & Biology*, vol. 63, no. 13, p. 135 023, 2018.

[109] E. Zastrow, S. C. Hagness, and B. D. Van Veen, "3d computational study of non-invasive patient-specific microwave hyperthermia treatment of breast cancer", *Physics in Medicine & Biology*, vol. 55, no. 13, p. 3611, 2010.

[110] B. Guo, L. Xu, and J. Li, "Time reversal based microwave hyperthermia treatment of breast cancer", *Microwave and Optical Technology Letters*, vol. 47, no. 4, pp. 335–338, 2005.

[111] H. D. Trefná, J. Vrba, and M. Persson, "Time-reversal focusing in microwave hyperthermia for deep-seated tumors", *Physics in Medicine & Biology*, vol. 55, no. 8, p. 2167, 2010.

[112] J.-L. Thomas and M. A. Fink, "Ultrasonic beam focusing through tissue inhomogeneities with a time reversal mirror: Application to transskull therapy", *IEEE Transactions on Ultrasonics, Ferroelectrics, and Frequency Control*, vol. 43, no. 6, pp. 1122–1129, 1996.

[113] M. Fink, G. Montaldo, and M. Tanter, "Time reversal acoustics", in *IEEE Ultrasonics Symposium, 2004*, IEEE, vol. 2, 2004, pp. 850–859.

[114] G. Lerosey, J. De Rosny, A. Tourin, A. Derode, G. Montaldo, and M. Fink, "Time reversal of electromagnetic waves", *Physical review letters*, vol. 92, no. 19, p. 193 904, 2004.

[115] P. Takook, H. D. Trefná, A. Fhager, and M. Persson, "Evaluation of the 3D time reversal method for hyperthermia treatment planning in head and neck tumors", in *2015 9th European Conference on Antennas and Propagation (EuCAP)*, IEEE, 2015, pp. 1–5.

[116] N. Leduc, K. Okita, K. Sugiyama, S. Takagi, and Y. Matsumoto, "Focus control in HIFU therapy assisted by time-reversal simulation with an iterative procedure for hot spot elimination", *Journal of Biomechanical Science and Engineering*, vol. 7, no. 1, pp. 43–56, 2012.

[117] M. Zanoli and H. D. Trefná, "Iterative time-reversal for multi-frequency hyperthermia", *Physics in Medicine & Biology*, 2020.

[118] M. Seebass, R. Beck, J. Gellermann, J. Nadobny, and P. Wust, "Electromagnetic phased arrays for regional hyperthermia: Optimal frequency and antenna arrangement", *International Journal of Hyperthermia*, vol. 17, no. 4, pp. 321–336, 2001.

[119] M. M. Paulides, J. F. Bakker, A. P. Zwamborn, and G. C. Van Rhoon, "A head and neck hyperthermia applicator: Theoretical antenna array design", *International journal of hyperthermia*, vol. 23, no. 1, pp. 59–67, 2007.

[120] P. Togni, Z. Rijnen, W. Numan, R. Verhaart, J. Bakker, G. Van Rhoon, and M. Paulides, "Electromagnetic redesign of the hypercollar applicator: Toward improved deep local head-and-neck hyperthermia", *Physics in Medicine & Biology*, vol. 58, no. 17, p. 5997, 2013.

[121] J. Vrba, M. Lapeš, and L. Oppl, "Technical aspects of microwave thermotherapy", *Bioelectrochemistry and bioenergetics*, vol. 48, no. 2, pp. 305–309, 1999.

[122] J. Yang and A. Kishk, "A novel low-profile compact directional ultra-wideband antenna: The self-grounded bow-tie antenna", *IEEE Transactions on Antennas and Propagation*, vol. 60, no. 3, pp. 1214–1220, 2011.

[123] P. Takook, M. Persson, J. Gellermann, and H. D. Trefná, "Compact self-grounded bow-tie antenna design for an uwb phased-array hyperthermia applicator", *International Journal of Hyperthermia*, vol. 33, no. 4, pp. 387–400, 2017.

[124] G. G. Bellizzi, M. M. Paulides, T. Drizdal, G. C. van Rhoon, L. Crocco, and T. Isernia, "Selecting the optimal subset of antennas in hyperthermia treatment planning", *IEEE Journal of Electromagnetics, RF and Microwaves in Medicine and Biology*, vol. 3, no. 4, pp. 240–246, 2019.

[125] M. Zanoli and H. D. Trefná, "Optimization of microwave hyperthermia array applicators using field interpolation", in *2019 IEEE International Symposium on Antennas and Propagation and USNC-URSI Radio Science Meeting*, IEEE, 2019, pp. 537–538.

[126] J. Lagendijk, G. Van Rhoon, S. Hornsleth, P. Wust, A. De Leeuw, C. Schneider, J. Van Ddk, J. Van Der Zee, R. V. Heek-Romanowski, S. Rahman, *et al.*, "Esho quality assurance guidelines for regional hyperthermia", *International journal of hyperthermia*, vol. 14, no. 2, pp. 125–133, 1998.

[127] R. Canters, M. Franckena, M. Paulides, and G. Van Rhoon, "Patient positioning in deep hyperthermia: Influences of inaccuracies, signal correction possibilities and optimization potential", *Physics in Medicine & Biology*, vol. 54, no. 12, p. 3923, 2009.

[128] M. Zanoli, M. Persson, and H. D. Trefná, "Self-calibration algorithms for microwave hyperthermia antenna arrays", 2018.

[129] R. C. Conceição, J. J. Mohr, M. O'Halloran, *et al.*, *An introduction to microwave imaging for breast cancer detection*. Springer, 2016.

[130] P. Hashemzadeh, A. Fhager, and M. Persson, "Experimental investigation of an optimization approach to microwave tomography", *Electromagnetic biology and medicine*, vol. 25, no. 1, pp. 1–12, 2006.

[131] P. M. Meaney, T. Zhou, M. W. Fanning, S. D. Geimer, and K. D. Paulsen, "Microwave thermal imaging of scanned focused ultrasound heating: Phantom results", *International Journal of Hyperthermia*, vol. 24, no. 7, pp. 523–536, 2008.

[132] M. Haynes, J. Stang, and M. Moghaddam, "Real-time microwave imaging of differential temperature for thermal therapy monitoring", *IEEE Transactions on Biomedical Engineering*, vol. 61, no. 6, pp. 1787–1797, 2014.

[133] M. G. Aram, L. Beilina, and H. D. Trefná, "Microwave thermometry with potential application in non-invasive monitoring of hyperthermia", *Journal of Inverse and Ill-posed Problems*, vol. 1, no. ahead-of-print, 2020.